Geometrical metrology on vacuum cast silicone rubber form using computed tomography

Pacurar, Ramona; Müller, Pavel; De Chiffre, Leonardo

Publication date:
2011

TECHNICAL REPORT

Geometrical metrology on vacuum cast silicone rubber form using computed tomography

RAMONA PĂCURAR

PAVEL MÜLLER

2011

UNIVERSITATEA TEHNICĂ DIN CLUJ-NAPOCA (UTCN)

DANMARK TEKNISKE UNIVERSITET (DTU)

GEOMETRICAL METROLOGY ON VACUUM CAST SILICONE RUBBER FORM USING COMPUTED TOMOGRAPHY

Authors RAMONA PĂCURAR

PAVEL MÜLLER

Supervisor LEONARDO DE CHIFFRE

Contents

FOREWORD

This project is a result of an external stay at the Department of Mechanical Engineering – DTU Mekanik, Technical University of Denmark, in the period from September to December 2010, under the supervision of Prof. Dr. Eng. Leonardo De Chiffre. This work was carried out in collaboration with the Department of Manufacturing Engineering from the Technical University of Cluj-Napoca, Romania under the supervision of Prof. Dr. Eng. Petru Berce (TUCN).

The authors would like to thank René Sobiecki for performing all the measurements on CMM and also to Danish Technological Institute (DTI) for collaboration and for measurements performed on the CT scanner.

ABSTRACT

An investigation on geometrical measurements of silicone rubber cake form and polyamide molds using three measuring techniques - CMM, optical scanner and CT scanner - was carried out. The only measurand was diameter of a cone measured at specified levels. An uncertainty budget for all three techniques was assessed and expanded combined uncertainties calculated. The measurements on CMM were considered as reference measurements.

When measuring silicone rubber form, this was supported by the molds due to its the high flexibility. Investigation on deformation effect of the silicone rubber cake form and the molds was carried out. It was found that the higher probing force was used, the smaller coefficient of variation was obtained. This means that higher reproducibility was achieved when higher probing force was applied.

Two measuring strategies on CMM were realized: Single point probing (SPP) and probing in scanning mode (SMP). It was found that SMP results in smaller data variability. However, the difference compared to SPP was not big and since SPP measuring strategy is generally used for measuring a big variety of parts, this was used for further comparisons between CMM and the other two measuring techniques.

It was found that when the silicon rubber form was measured on the supported bottom mold or the bottom mold was measured itself, the diameter measurements performed on optical scanner and CT scanner were bigger compared to CMM measurements. On the other hand, the diameter resulted in smaller values when the silicon rubber form was measured on the supported top mold or the top mold was measured itself.

A procedure for measurement of highly deformable part, such as silicone rubber form, was developed. Uncertainties from measurement on the optical scanner were big. This was mainly connected with low reproducibility of scanning individual positions of the cone. Measuring uncertainties for CT measurements were calculated in a range which is reasonable when considering such deformable sample. Therefore, CT scanning is highly recommended measuring technique, resulting in short measuring times and measuring of complicated features. In connection with the silicone rubber form, CT scanning could be also used for example for failure analysis, 3D volume analysis and other non-destructive and metrological analysis.

AIM OF THE WORK

The aim of this project was to perform dimensional and geometrical measurements on silicone rubber cake forms and polyamide molds, and calculate the uncertainty of all the measurements from different measuring instruments (tactile CMM, optical CMM and CT scanner). The reference measurements on CMM ensure traceability of the measurements.

Chapter 1

GEOMETRICAL METROLOGY ON VACUUM CAST SILICONE RUBBER FORMS

1.1 INTRODUCTION

Geometrical metrology is a technical discipline where dimensional and geometrical measurement of workpieces belongs to common measuring tasks in mechanical engineering. The aim is to verify tolerances and specifications defined on the technical drawings. It is important that the measurement traceability, controlling the correct function of a measuring instrument, is ensured and so the measurement results are traceable to the unit of meter. Traceability is generally achieved through calculating the task specific measuring uncertainty. CT scanners are however not traceable to the unit of meter. The assessment of equation for uncertainty calculation is a rather difficult task due to many influence factors in CT metrology. It is therefore necessary to compare measuring results from CT scanner with measurements performed for example using coordinate measuring machine (CMM), where traceability is known.

Generally, non-contact measuring techniques are needed when measuring soft materials. This is due to the fact, that no forces are applied on the workpiece and therefore no deformation of the part takes place.

The aim of this investigation was to perform dimensional measurements on a silicone rubber and compare the results with measurements using a 3D optical scanner and a CT scanner. The item under investigation is a cake form (ESSIL 291), which was produces by vacuum casting method. This method is one of the most used, interesting and spectacular applications for use of Rapid Prototyping (RP) models to develop new products.

1.2 REPORT STRUCTURE

The project report is structured as follows:

- A brief presentation of silicone rubber used to manufacture cake forms, especially chemical structure, technological advantages, applications, rubber types, contact times and temperature, etc. (Chapter 2).
- A brief presentation of vacuum casting method and process chain for cake form development (Chapter 3).
- Basics of three measuring techniques used in the present investigation: tactile CMM, optical and CT (Chapter 4).
- Measuring plan, setups and strategies for individual measuring techniques (Chapter 5).
- Uncertainties assesment for measurements on CMM, optical scanner and CT scanner (Chapter 6).
- Comparison of the results obtaied with CMM, optical scanner and CT scanner (Chapter 7).

Chapter 2

SILICONE RUBBER

This chapter provides a brief presentation of silicone elastomers used to manufacture some cake forms to improve product quality, increase efficiency, reduce the time needed for hygenisation and to diminish the microbial load of the form.

2.1 INTRODUCTION

Silicone elastomers are used since the early 70s in medical, aerospace, electronics, auto industry, in construction as well as other industrial applications. These elastomers enjoy today a success due to their unique characteristics, such as increased compressive strength, flexibility in a large range of temperatures, a wide range of hardness (5-80 Shore A). Silicone rubber is a synthetic polymer with a molecular structure consisting of a huge chain formed by two atoms of silicon and oxygen in alternative way (Figure 2.1).

2.1.1 Chemical structure

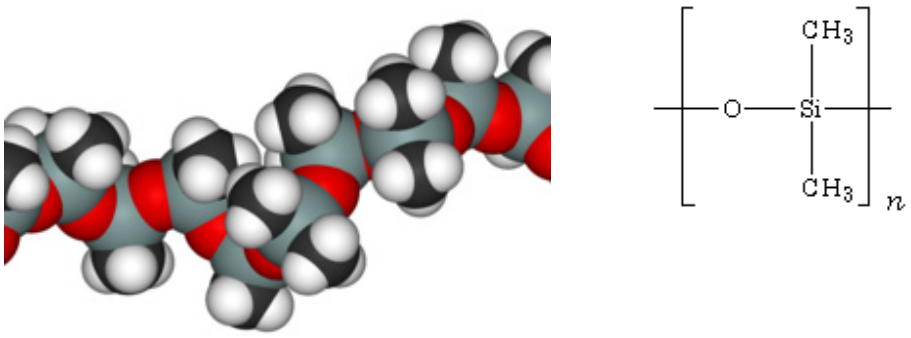

Figure 2.1: Silicone rubber chain [1].

The powerful link of silicon-oxygen gives silicone rubber its own performance and characteristics consisting in increased resistance to various chemical agents and variations in temperature, excellent mechanical and dielectric properties, biocompatibility, transparency and natural clarity.

2.1.2 Technological advantages of silicone rubber

- Light mixing and processing.
- Very small processing times, depending on thickness and geometry of the part walls.
- Easy removal from the mold.

- Injection without loss.
- In general, does not require post treatment.
- Adheres very well to certain materials.
- High clarity.
- Odorless and neutral taste.
- Usable in the range of temperatures – 50 °C ÷ + 250 °C.
- Excellent elastic properties.
- Very good resistance against the ultraviolet attack and the ozone exposure.
- Increased aging resistance.
- Natural rejection of water and resistance against the attack of various solvents.
- Excellent dielectric properties in a variable range of temperatures.
- Silicone rubber is not a fuel, it does not melt and doses not run.
- Toxicity of pollutants released is very low.

2.1.3 Liquid silicone rubber applications

- Automotive industry: sheets for spark plugs, various membranes, etc.
- Electronics: terminal elements, connectors, keyboards for computers and phones, diaphragms, etc.
- Home appliances and accessories: low insulation, membrane, different components for coffee makers, *cake forms*, etc.
- Medical accessories: catheters, teats and soothers, etc.
- Others: swimming glasses, diving masks, etc.

The rubber can be found in the following sectors of the food industry:

- Dairy and dairy products.
- Brewery and soft drinks.
- Abattoir and meat processors.
- *Confectionery producers and bakers.*
- Vending machine dispensers.
- Food canning and preserves industry.
- Pressure cooker seals.
- Breakfast cereal manufacturers.
- Food packaging.

2.1.4 Rubber types

One of the most important criteria which can be used in selection of a special rubber for a final utilization is its resistance to temperature, although other proprieties are also taken into account, such a chemical inertness, physical properties of the resulting product (tensile strength, abrasion and tear strength) on the side types of additives needed to be added into it to achieve desired processing and final properties. The most important types of rubber used in the food industry are:

- Natural rubber.
- Nitrile rubber.
- Ethylene-propylene rubber.
- Fluorocarbon rubber.

- *Silicone rubber.*
- Thermoplastic elastomers (TPE).
- Styrene-butadiene rubber (SBR).

2.2 TERMS OF USE FOR SILICONE RUBBER IN THE FOOD INDUSTRY (RUBBER PRODUCTS AND CONTACT TERMS)

2.2.1 Types of Rubber Products

a) b) c)

Figure 2.2: a) Silicone rubber cake forms; b) Hoses; c) Gaskets.

The main types of rubber products used in contact with food are shown below in Table 2.1.

Table 2.1: Examples of the rubber components used in food contact [2].

Location	Component(s)
Food transport	Belt-type carrier, hoses, rubber plinths
Pipes components	Gaskets, flexible connectors
Pumps	Pumps with diaphragm
Cans / bottles	Gaskets
Handling / Preparation of food products	Gloves
Food manufacture	*Sweet molds*, twisted
Food packaging	Meat netting and poultry meat

2.2.2 Contact times

Contact time with the individual rubber components tents to be low, less than 60 seconds and no more than 3 minutes for heat-exchanger. Some components or assemblies come into a longer contact with food products, exceptions are for the belt-type carrier and silicone rubber cake forms, where the contact time is less than one hour.

2.2.3 Contact temperature

When some rubber components come into contact with food the temperature rarely exceed 80°C. Temperatures between 100-140°C occur in some process like UHT milk pasteurization, caramels production in *silicone rubber forms*, canned and bottle sterilization but food contact time at high temperatures is, normally, reasonably short (<1 hour). An overall summary of data collected during the food industry investigations is illustrated in Table 2.2.

Table 2.2: Summary of the food industry investigations related to the rubbers in contact with food [2].

Component	Contact zone – individual components [cm^3]	Contact zone – assemblies of components [cm^3]	Proper contact times	Maximum contact times	Contact temperature	
					general [°C]	extreme [°C]
Food carrying	To 50,000	-	<1 hour	-	<85	-
Piping components	<1,000	<10,000	<1 hour	2 weeks	<140	250
Pumps	<10,000	-	<1 hour	2 weeks	<85	-
Gaskets	<1,000	To 30,000	<1 hour	12 weeks	<140	-
Miscellaneous	<1,000	-	<1 hour	4 weeks	<85	250

2.3 ESSIL 291

The material used for the manufacture of the transparent silicone rubber cake form, which has been used as a sample in this project, is ESSIL 291.This silicone rubber called Essil 291 is sold globally via the Axson Technologies Subsidiary Network directly to these markets. It is a silicone system with 3 catalyst options:

- 291 Catalyst - for dry moulds, typically used for high quality lens work. Shore A 38.
- 292 Catalyst - a controlled 'oil bleed' version to add de-mould lubrication. Shore A 38.
- 293 Catalyst - slightly higher shore hardness version of 291, for RIM tools. Shore A 40.

The catalyst used for the manufacture of this silicone rubber cake form was 291 Catalyst.

Being a low viscosity system, the resulting benefits to production are soon evident. The low viscosity discourages air entrapment when mixed, resulting in a quicker degas and release of air bubbles. Essil 291 demolds in 12 hours at 23°C but is usually cured at 40°C for this period.

Properties:

- High transparency
- Good chemical resistance towards polyurethanes
- Vulcanized by polyaddition
- Very easy to mix and to cast
- Very low shrinkage when hardening at room temperature

Physical and mechanical properties of Essil 291 at 23°C can be seen.

Table 2.3: Physical properties of Essil 291 [3].

			Essil 291 / Essil 291
Viscosity at 25°C	Brookfield LVT	MPs.s	40,000
Demolding time at 23 °C		hour	12
Demolding time at 70°C		hour	4
Color			transparent

Table 2.4: Mechanical properties at 23 °C of Essil 291 [3].

			Essil 291/ Essil 291
Hardness	ISO 868:2003	Shore A1	38
Tensile strength	ASTM D412:1997	MPa	5
Elongation at break	ASTM D412:1997	%	350
Tear strength	ASTM D624:1992	KN/m	24
Coefficient of linear expansion	-	10^{-4} .K $^{-1}$	3
Linear shrinkage	-	%	< 0.1
Linear shrinkage after curing at 70°C (curing after gel)	-	%	< 0.7

Note: Average values obtained on standard specimens after hardening 7 days at room temperature.

Chapter 3

VACUUM CASTING

This chapter provides a brief presentation of vacuum casting method including the equipment used for casting silicone rubber and also the steps needed for manufacturing of the molds and of the transparent silicone rubber cake form.

3.1 VACUUM CASTING

Vacuum Casting is the method used for obtaining silicone rubber molds. This method is one of the most used, interesting and spectacular applications for use of Rapid Prototyping (RP) models to develop new products. Vacuum Casting is a technique that has proved the appropriateness and efficiency in the stage of developing new products, step when prototyping of complex parts must be used for small batches (30-50 parts), for testing new product functionality and/or market testing of the new product.

This manufacturing method reproduces faithfully the details of form and the quality of RP model surfaces used as a master.

Materials used in the vacuum casting are different types of resins, plastics and rubber.

3.2 EQUIPMENT PRESENTATION

The Center for Rapid Prototyping of the Technical University of Cluj-Napoca is using a vacuum casting machine type MCP-001 PLC, which is shown in Figure 3.1. The manufacturing of the form is performed using silicon-type ESSIL 291. This silicone can be used with one of the following 3 catalysts:

- ESSIL 291 - for dies which are not using a lubricant, Shore hardness A 38 – this is used in the Technical University of Cluj-Napoca.
- ESSIL 292 - for products extraction from molds with a lubricant, Shore hardness A38.
- ESSIL 293 - 291 version with high hardness Shore A40.

Figure 3.1: Vacuum Casting machine MCP-001 PLC at TUCN.

The present investigation was carried out using this vacuum casting machine to manufacture silicone rubber form intended to be used in food industry as a cake form. The materials used in manufacturing were silicone rubber type ESSIL 291 and catalyst type ESSIL 291 (see Section 2.3).

3.3 PROCESS CHAIN FOR CAKE FORM DEVELOPMENT

The steps needed for casting silicone rubber form for the food industry are:

1. **Developing a CAD drawing of the cake form**. This form is intended for the production of cakes. As it can be seen below in Figure 2 desired form has four different types of cavities.

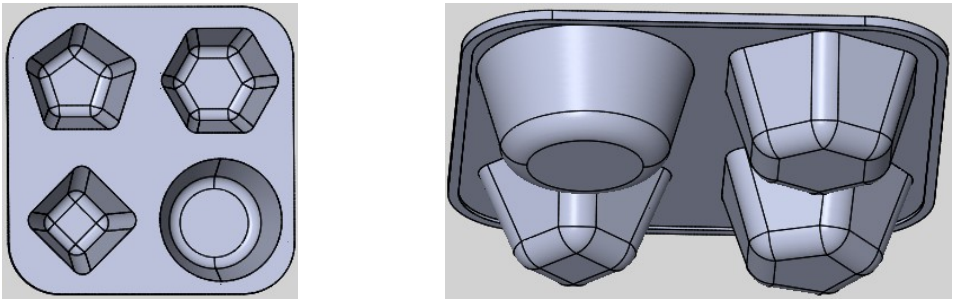

Figure 3.2: CAD drawing of the cake form.

2. **Manufacture of the bottom and top molds.** The molds were manufactured using Haas Milling Machine at the Technical University of Cluj-Napoca, which is shown in Figure 3. The material used in this step was a polyamide A6.

Figure 3.3: Haas Milling Machine at TUCN.

Individual steps in mold manufacturing can be seen in Figure 3.4 (a, b, c, d). The final products, namely molds are shown in Figure 3.5 and Figure 3.6.

3. **Preparation of the silicone rubber** to be casted between the top and bottom mold. In this step, the mixing of the two components, silicone rubber and catalyst, is taking place. Before the casting, silicone rubber is introduced in a vacuum chamber for de-gassing.

4. **Getting the silicone rubber form** by casting silicone rubber between the top and bottom polyamide molds with the funnel formed in the bottom mold. Two types of silicone rubber were tested. Figure 3.7 shows the casting step for white silicone rubber and Figure 3.8 shows the casting step for transparent silicone rubber. Due to high viscosity of the silicone rubber, pressure on silicone was applied, because it has slow flow (Figure 3.9).

5. After casting between the molds, the assembly is introduced in the vacuum chamber **to eliminate the air bubbles** accumulated during the casting.

6. For the solidification of silicone rubber cast in the previous stage, the whole assembly is introduced in the polymerization oven at about 70°C, for about 2-3 hours.

7. By opening the two polyamide molds, the food silicone rubber form (Figure 3.10) can be detached and subsequently used to produce cakes.

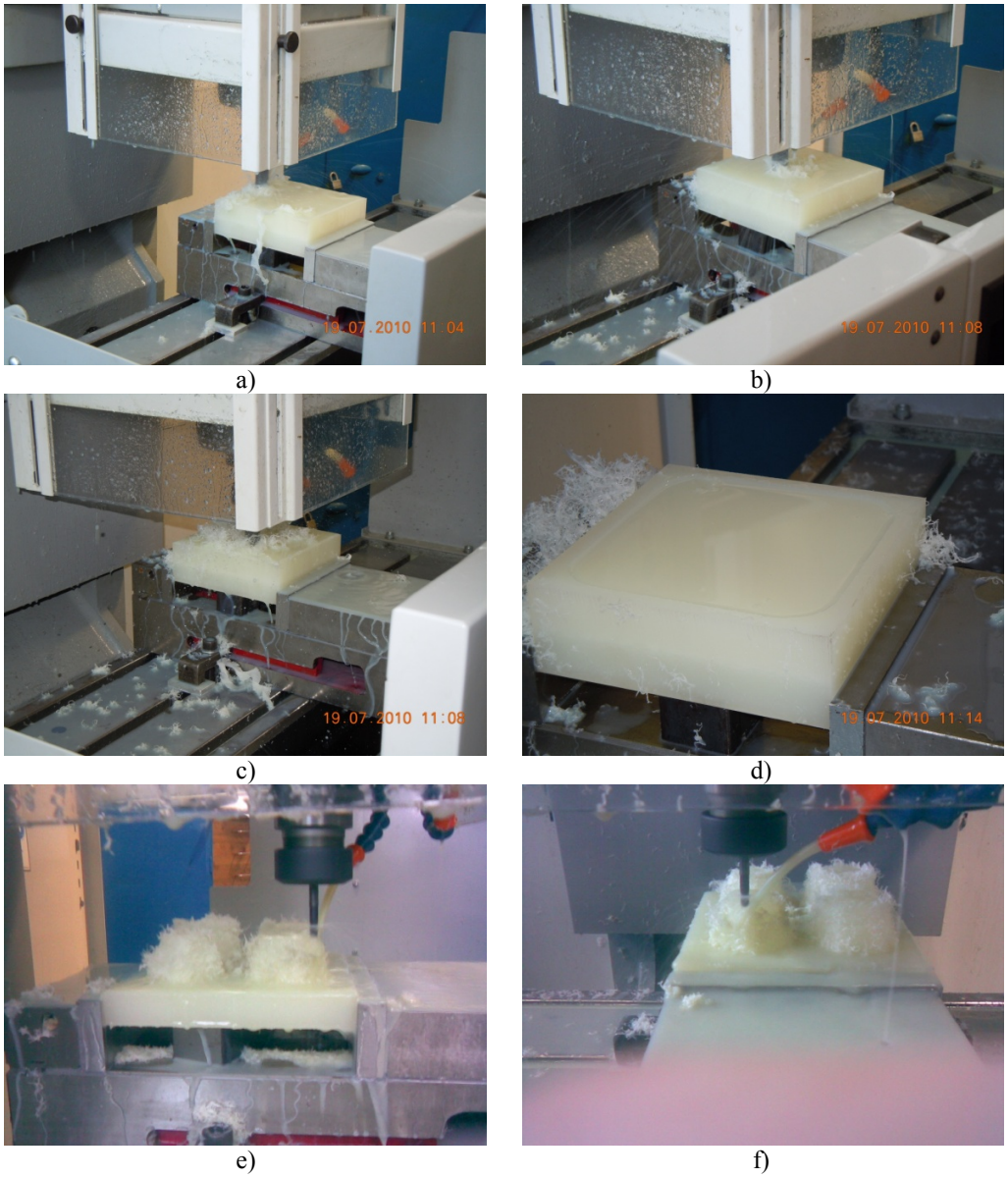

a) b) c) d) e) f)

Figure 3.4: Individual steps in molds manufacture using Haas Milling Machine at TUCN (a, b, c, d, e, and f).

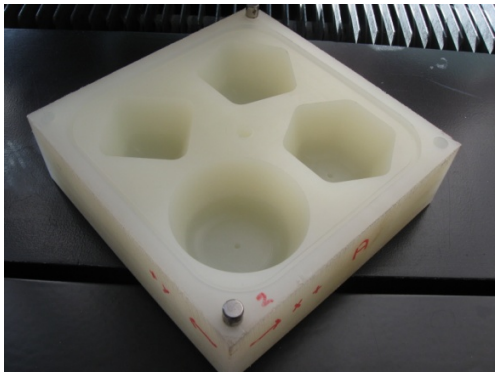

Figure 3.5: Polyamide Bottom mold A.

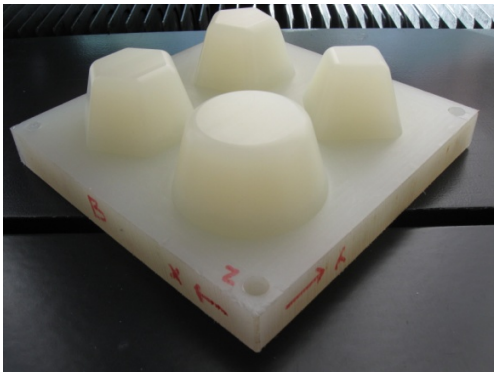

Figure 3.6: Polyamide Top mold B.

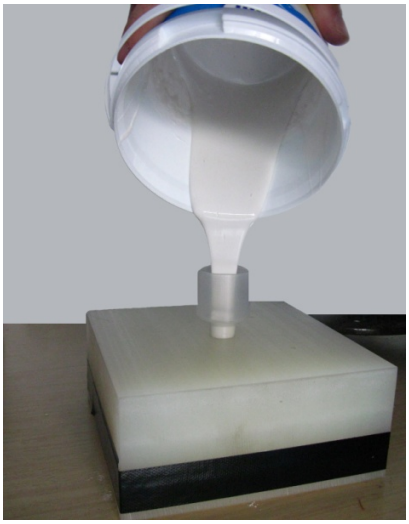

Figure 3.7: Casting of white silicone rubber.

Figure 3.8: Casting of transparent silicone rubber.

Figure 3.9: Application of a manual pressure.

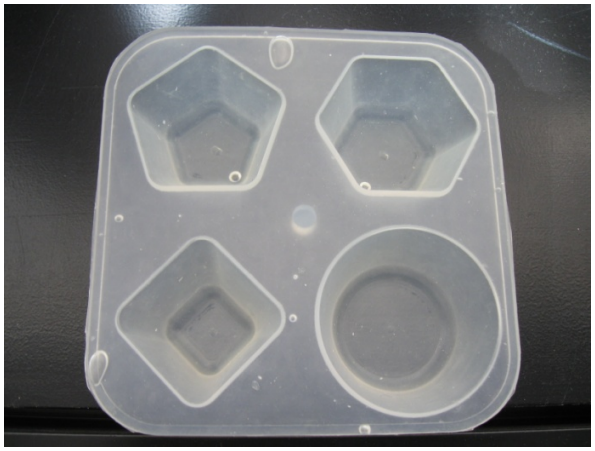

Figure 3.10: Silicone rubber form for cakes.

Chapter 4

MEASUREMENT TECHNIQUES

This chapter describes different measuring technologies which have been used in the present investigation. Each technology has its own advantages and disadvantages, which are also discussed.

The three measuring instruments used in the present investigation are:

- Tactile CMM: UPMC 850 Carat, Zeiss
- Optical scanner: Hawk DS 100, Nextec
- CT scanner: Metrotom 1500, Zeiss

4.1 MECHANICAL PROBING USING COORDINATE MEASURING MACHINES (CMMs)

4.1.1 Introduction

Coordinate measuring machines (CMMs) are the most important general-purpose instruments for the measurement of mechanical workpieces in industry. CMMs are well accepted in industry because they are very flexible and allow the measurement of points in space with high accuracy. They are typically provided with numeric control and scanning probes, both contact and non-contact; automatic measurements of thousands of points are easily performed, even on complex surface [4]. CMMs are widely used because of their flexibility, and are found in many different roles in the chain of quality assurance in companies. Some of these applications are:

1. Inspection of workpieces (post- and in-process).
2. Process-capability studies.
3. Control of tools.
4. Measurements during product development.
5. Measurement of models and prototypes.
6. Calibration of gauges and master workpieces.

For all these applications there is one common requirement: the measurement results must be traceable to the unit ‘meter’ and uncertainties must be stated. Only traceable measurements are valid for certified or accredited quality assurance systems [4].

4.1.2 Basics of coordinate metrology

Coordinate metrology using CMMs is basically a question of collecting single points on the surface of a workpiece. The probed points are all represented by the coordinates (X, Y, Z) (Cartesian coordinate system presumed). These coordinates do not give any information as to the parameters (diameter, angle, etc.) of the

workpiece under investigation. Therefore the points have to be combined into substitute geometric elements by applying mathematical algorithms to combinations of single points. The number of sampled points necessary to perform the calculation of the substitute geometric element depends on the geometry [4].

A CMM consists of the following main elements:

- Mechanical layout of the axes
- Displacement transducers for the axes
- Probing system
- Control unit and computer with software for control of the CMM and data evaluation.

The mechanical layout of the axes is the physical representation of the coordinate system, and the movements are performed along these axes. The displacement transducers convert the actual position of the guideways into length units in the coordinate system. The probing system is the link between the workpiece and the CMM. In the case of a mechanical probing system the probing is performed by a mechanical contact between stylus and workpiece. The control unit controls the movement of the guideways and the probing system according to the commands of the operator of the CMM. The interface between the CMM and the operator is the computer and the software of the manufacturer of the CMM. The software contains algorithms for calculation of the substitute geometric elements as well as computer control for automatic measuring cycles of the CMM (CNC programming).

The control unit of the CMM, in co-operation with the digital computer and the measuring software, take care of the control of the machine. This can be done either manually or through the use of computer numerical control (CNC). The software also performs the calculation of substitute geometric elements and evaluation of the results. These calculations are based upon input from the operator of CMM.

A CMM's main components are:

- Air bearing on granite guideway
- Grating scale for Y axis (measuring scale)
- Probe configuration
- Measuring head
- CMM bridge travel
- Output screen
- Control unit
- Control panel
- Granite plane
- Passive isolator system [4].

4.1.3 Classification of CMM configurations

CMMs can be of different construction using different lay-outs of the axes, can have different number of axes, different types of coordinate systems, etc. Table 4.1 presents the most common types of CMM configuration [4].

Table 4.1: The most common CMM configurations [5-8].

Types of CMM configuration		
Bridge CMMs	a) Moving bridge	b) Fixed bridge
		
Cantilever CMM		
Horizontal arm CMM		
Gantry CMM	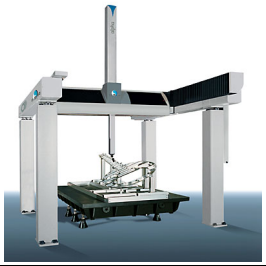	

The **UPMC 850 CARAT** machine at Technical University of Denmark (DTU) is of a type Moving Bridge [4]. The most important components are:

- Stationary table to support the workpiece to be measured.
- Most widely used configuration.
- High table-load capacity.
- Low bending effect of the horizontal axis.
- Two columns move at different paces causing bridges twist.
- CMM's accuracy depends on measuring location on the CMM table.

4.1.4 Contact probing systems

The probing system of a CMM may be mechanical or optical. Mechanical probing systems are usually divided into touch-trigger systems (dynamic probing systems) and the three-dimensional measuring probe systems (static probing systems) [4].

The **UPMC 850 CARAT** CMM at DTU is equipped with a static probe. The static probing system can measure without relative motion between probe and workpiece. In general, it is more accurate than the dynamic probing system. Positioning control can act in one, two or three axes simultaneously. Data from both probe head and CMM linear scales are added in all three measuring axes. The static probe allows measurements in both point-to-point and continuous scanning mode. During scanning, the control system continuously repositions the probe head in the probing axis, remaining within its measuring range with virtually constant measuring force. Deflection is measured and taken into account. In scanning mode, high density acquisition of measurement points is possible. Scanning is important for form measurement [4].

Figure 4.1: Coordinate Measuring Machine UPMC 850 CARAT at DTU.

Error sources connected to CMM are summarized in Figure 4.2.

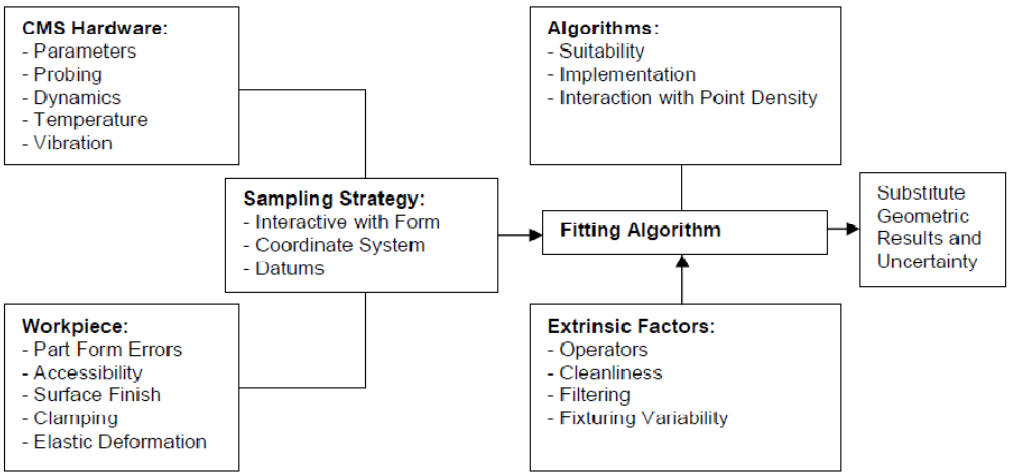

Figure 4.2: Error components for contact probing techniques [9].

4.2 OPTICAL TECHNIQUES

4.2.1 Introduction

Optical scanning metrology is using a non contact probing techniques for obtaining three-dimensional (3D) scans of the objects to be measured. It involves a digitization process that acquires geometrical information on the surface of an object. One of the main advantages of non contact measuring techniques with respect to mechanical ones is measuring speed. Compared to mechanical CMMs, non contact techniques can typically acquire more data in shorter time. The dense point clouds acquired can be directly compared to a nominal CAD model and the operator can see instantly where a part is in or out of tolerance. Other important advantages of non contact techniques are the possibility to measure without contacting the part and the easier access to details that are difficult to be probed mechanically. Flexible or delicate parts can be digitized without problems, while a mechanical probing system could deform the surface due to the probing force (e.g. the transparent silicone rubber form) [4].

The uncertainty for non contact technologies is however not assured, being as least one order of magnitude higher than the corresponding contact probes. CMMs are currently the leadership for quality control processes of industrial parts in the scope of contact technology. This is due to the fact that calibration process and the uncertainty in measurements are the well-known [10].

4.2.2 Principle of Optical 3D scanner

Triangulation principle: A light spot or stripe is projected onto an object surface and the position of the spot on the object is recorded by one or more CCD cameras. The angle of the light beam leaving the scanner is internally recorded and the fixed base length between laser source and camera is known from calibration. The distance from the object to the instrument is geometrically determined from the recorded angle and base length (Figure 4.3).

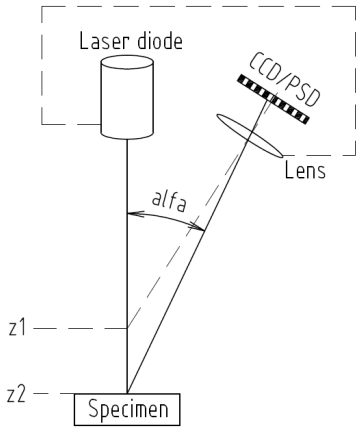

Figure 4.3: Triangulation principle: single camera solution.

4.2.3 Instrument presentation

Technical University of Denmark (DTU) is using a 3D optical scanner type Hawk DS 100 from Nextec (Figure 4.4). The measuring volume in [X, Y, Z] is [240, 240, 240] mm.

Figure 4.4: Optical 3D scanner Hawk DS 100 from Nextec at DTU.

The Hawk provides a turnkey solution for rapid scanning and digitizing of three-dimensional surfaces. The Hawk is equipped with the WIZprobe, which combines the latest in laser technology with fast and accurate scanning. The WIZprobe uses the standard triangulation method.

Complex free form shapes can now be rapidly reconstructed, reproduced, and verified by utilizing the Hawk's power and flexibility. During the scanning process, the system records and displays the numerical data in real time. This high-density data can be exported into a CAD/CAM system for further processing and CAD model comparison.

The Nextec Hawk system is comprised of the following components:

- *WIZprobe.* The WIZprobe is a non-contact optical laser-scanning sensor for making geometric scans.
- *Hawk Software.* The Hawk includes its own Windows NT software that has been specifically developed to implement the operation of the machine. The operator uses the software to set the scan parameters and to view and export data.
- *3D motion platform.* The 3D motion platform consists of an XY motion stage where the part to be measured is mounted, a Z axis arm which moves the WIZprobe, and an electrical cabinet which houses the controllers and the power supply.

Summary of the influence factors in an optical measurement can be seen in Figure 4.5.

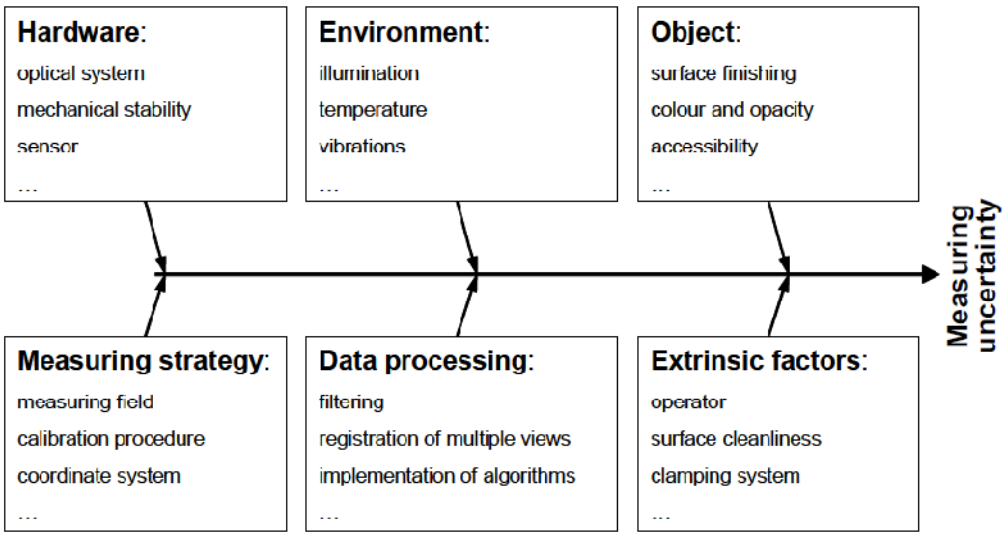

Figure 4.5: Summary of factors that influence the accuracy of optical systems [11].

4.3 COMPUTED TOMOGRAPHY (CT)

4.3.1 Introduction

Computed tomography (CT), also called CT scanning, is a non-destructive measuring technique, allowing inspection of internal and external geometries of a workpiece. CT is used in many industrial fields (material science, electronics, military, medical, food, security, aerospace and automotive) [12-14]. Few years ago CT has become an important player in the field of coordinate metrology. CT is in a relatively short time capable to produce a complete three-dimensional model of the scanned part. One of the biggest advantages of using CT compared to other measuring technique, like tactile measuring techniques, is the high density of points acquired on the scanned part. A key issue in using CT scanning is that CT systems are not traceable to the unit of meter and evidence of many influence quantities due to which assessment of uncertainty is rather a challenge.

4.3.2 Principle of CT scanning

A typical CT scanner consists of an X-ray source, a rotary table, an X-ray detector and a data processing unit for computation, visualization and analysis of measurement results. CT scanning technique is distinguished between 2D-CT (see Figure 4.6a) and 3D-CT (see Figure 4.6b) depending whether a line or flat detectors are used respectively. In 2D-CT, a coupled translation of source and detector is necessary as the object is measured successively in thin slices. This sequence of rotation and translation is repeated depending on number of slices which have to be reconstructed. In the case of 3D-CT, objects which fit entirely into the cone beam can be measured with just one revolution of the rotary table. A linear translation of source and detector is not necessary. This is why 3D-CT offers speed advantages compared to 2D-CT. CT creates cross section images by projecting a beam of emitted photons through one plane of an object from defined angle positions performing one revolution. As the X-rays (emitted photons) pass through the object, some are absorbed, some are scattered, and some are transmitted. A process of X-ray intensity reduction, corresponding to those X-rays that are scattered or absorbed, is called attenuation. X-rays which are attenuated due to the interactions with the object will not reach the X-ray detector. Photons transmitted through the object at each angle are computed and visualized by computer creating a complete

reconstruction of the scanned object. The 3D gray value data structure gained in this way represents the electron density distribution in the measured object.

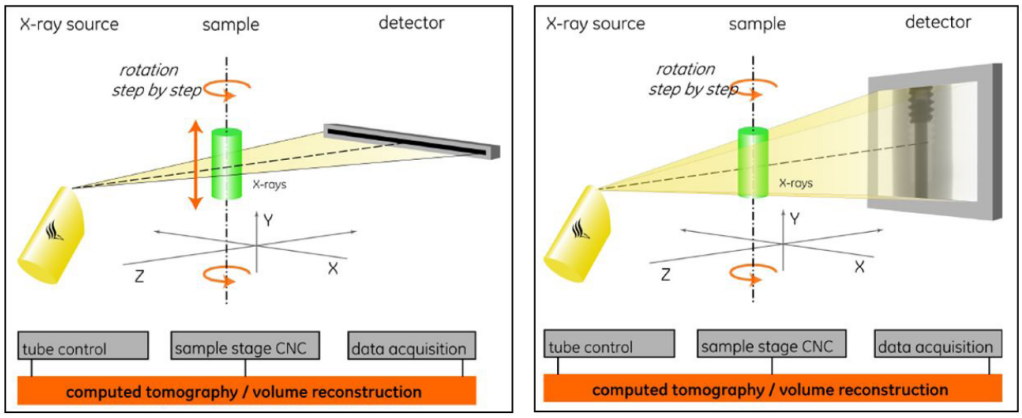

a) 2D-CT using linear detector b) 3D-CT using area detector

Figure 4.6: Principle of industrial CT [source: Phoenix X-ray].

CT application field has recently been broadened to include dimensional metrology. CT enables measuring the objects outside as well as the inside (e.g. invisible holes) in a non-destructive way. The ability to measure the inside of a part makes industrial CT attractive and unique in the world of dimensional metrology. Assemblies, complex structures as well as the inner geometry of parts made by rapid manufacturing can be measured in a non-destructive way.

4.3.3 CT scanner - METROTOM 1500

Danish Technological Institute (DTI) uses a CT scanner METROTOM 1500 from ZEISS (Figure 4.7).

Figure 4.7: CT scanner ZEISS METROTOM 1500 at DTI.

Using this CT scanner A big variety of materials can be scanned, depending on cumulative material thickness and composition. The most relevant materials scanned are specified below and can be seen in Figure 4.8.

- Plastics up to 250 mm thick.

- Light metal alloys up to 120 mm thick (Al, Mg).
- Model construction materials up to 200 mm thick (plaster, wood, bakelite, resin and sand cores).
- Ceramics and compound materials (depending on the density, porosity and composition).
- Steel (Metrotomography up to 10 mm, defect checks up to 15/18 mm).

Figure 4.8: Typical parts scanned on METROTOM 1500 [15].

Table 4.2: Metrotom's performance features [15].

Performance Features	
Tube power	5-1000 µA
Voltage	10-225 kV / 225 W / 225 keV
Detector	1024 x 1024 Pixels at 400 μm^2
Optional	2048 x 2048 Pixels at 400 μm^2
Measuring Range	Ø300 x 350 mm
Source-Detector Distance	1500 mm
Focal spot size	> 7 µm

4.3.4 Factors influencing CT performance

In order to quantify the accuracy of measurements using Computer Tomography, one has to identify the error sources. Figure 4.9 classifies the most important factors influencing CT performance using the basic components of the CT system as a starting point.

- *X-ray Source*

The factors related to the X-ray source are partly determined by the machine, but also partly to be chosen by the operator. The X-ray tube voltage can be chosen by the operator within a machine specific range. The higher the voltage, the more penetrating the X-ray beam becomes. The applied current is a user-defined input as well, which affects the intensity of the beam (i.e. the quantity of radiation energy).

Another important quantity is the focal spot size. Figure 4.10 illustrates the effect induced by the spot size. The smaller the spot size, the sharper the edges will be. In case of large spot sizes unsharpness will occur, known as the penumbra effect. A disadvantage of a smaller spot size is the concentrated heat produced at the spot on the target inside the X-ray tube, requiring cooled targets and limiting the maximum applicable voltage.

Other influencing factors are the target material and type (reflective or transmission target), the X-ray spectrum. The polychromatic character of conventional X-ray sources causes the well known effect of beam hardening: while the X-ray beam penetrates material, the low-energy X-rays (soft X-rays) are more easily attenuated than the higher-energy X-rays. As a consequence the image on the detector differs from the expected image,

resulting in observable errors in the reconstructed volume. The amount of beam hardening depends on the initial X-ray spectrum as well as on the composition, density and the amount of material traversed. One way to reduce beam hardening is to place a thin sheet filter in front of the workpiece in order to absorb the low energy radiation from the spectrum, hence approximating a more monochromatic energy distribution. Disadvantages are the loss of intensity with corresponding reduction of the signal-to-noise ratio due to a limited dynamic range of the detector and inadequate results in case of multi-material objects.

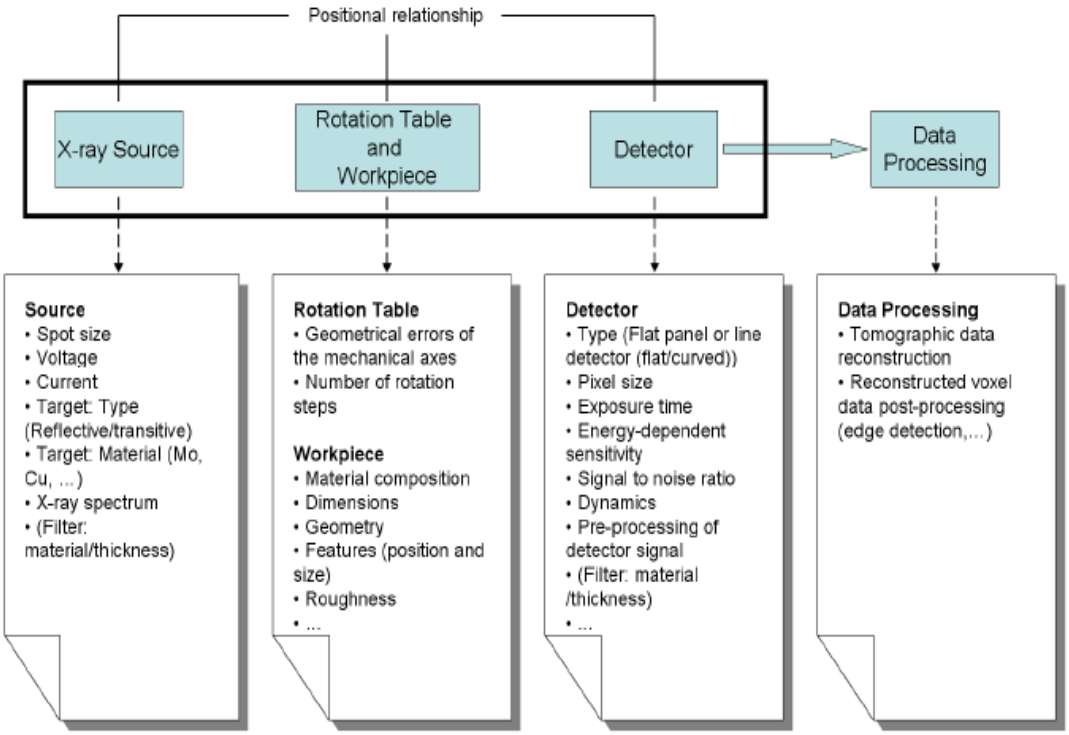

Figure 4.9: Classification of factors influencing the CT performance [16].

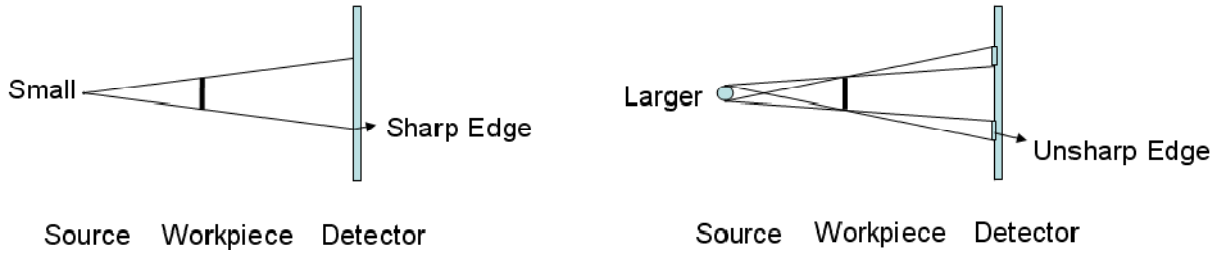

Figure 4.10: Small spot size (left) compared to large spot size (right) [16].

- *Rotation Table and Workpiece*

Since CT implies a reconstruction of X-ray images taken at different orientations, the workpiece is mounted on a rotation table. Influencing factors of this rotation table are the geometrical errors of the mechanical axes and the number of rotation steps chosen by the operator. Also workpiece characteristics including e.g. material composition and dimensions influence the accuracy of the CT results.

- *Detector*

Two types of detectors can be distinguished: 2D flat panel detectors and 1D line detectors. When using a flat panel detector, a single rotation of the object normally suffices, provided the detector is sufficiently large (in combination with restricted magnification). For line detectors, the rotation of the object should be complemented with an additional vertical displacement for every slice to be measured (e.g. 10,000 shifts of 10 μm for a 100 mm workpiece with 10 μm resolution). Consequently, the use of a line detector is more time consuming. Line detectors may however accommodate higher beam power (i.e. thicker objects) and better accuracy. A recent possibility (yet, since long applied in the medical world) is the use of a helix CT, where the workpiece makes a helical movement [17]. Other important detector characteristics include pixel size, number of pixels, exposure time and signal-to-noise ratio.

- *Data Processing*

Processing the detector output consists of two steps: reconstruction of the 2D images into a 3D voxel model, followed by the actual measurements (including determination of the edges, thresholding). While discussing the drawbacks of the polychromatic character of the X-ray source above, the problem of beam hardening was already mentioned: without appropriate corrections, beam hardening results in observable errors in the reconstructed volume. Another problem related to the reconstruction is X-ray scattering: as the X-ray beam passes through material some of the original energy in the beam can be deflected onto a new path. The effect changes with each projection resulting in artifacts in the reconstructed image.

- *Positional Relationship*

The distances between the detector, X-ray source and workpiece have a great influence on the accuracy of the CT measurements. A geometrical magnification is achieved by positioning the object close to the source. As a result more pixels of the detector are used, theoretically improving the resolution. However, at the same time the image becomes more blurred annihilating part of the benefit: A smaller distance between the source and the workpiece results in less parallel X-ray beams and a larger penumbra effect (i.e. less sharp edges) [16].

Chapter 5

MEASURING PLAN, SETUPS AND STRATEGIES FOR INDIVIDUAL TYPES OF MEASURING TECHNIQUES

This chapter is dedicated to the experimental part, including the test plan, description of different measurement setups and measuring strategies for individual measuring techniques. This chapter also describes investigation on force measurements performed on CMM which is a prerequisite for ensuring traceability of measurements on the CMM. This is mainly due to the big deformation of the silicon rubber form due to its elasticity.

The experiments were carried out at CGM, DTU laboratories and DTI.

5.1 INTRODUCTION

The samples investigated were two polyamide molds and one transparent silicone rubber cake form. The molds were also used as a support during measurements. The nomenclature of different samples is presented in Table 5.1.

Measurements performed on the CMM are considered to be reference measurements. This is due to the fact that measurements performed using contact technology result in better precision, higher repeatability and ensures traceability of the measurement.

The only feature measured and evaluated was the cone of the form and the cone of the two molds, see Figure 5.1. Diameters at different levels on the cone were measured.

First, an investigation on the influence of probing force on deformation of the material during measurements was carried out on CMM. This was done in order to evaluate the deformation effect. This will allow for correcting measurements when selected features of individual samples were measured.

Two different types of measurement comparisons were performed. First comparison considers a measurement performed on tactile CMM (tactile measurement) and optical scanner (optical measurement), second comparison considers measurement performed on tactile CMM and CT scanner.

Table 5.1: Nomenclature of scanned items.

Description	Image	Abbreviation used in the report
Bottom mold	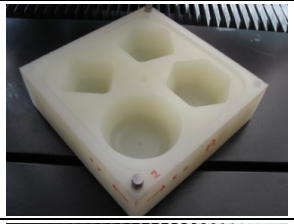	Mold A
Top mold		Mold B
Transparent silicone rubber form		Form
Transparent silicone rubber form on the bottom mold	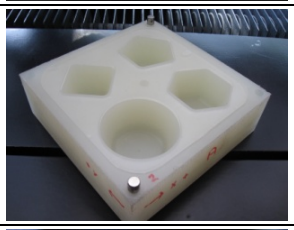	Form on A
Transparent silicone rubber form on the top mold		Form on B
White silicone rubber		White form

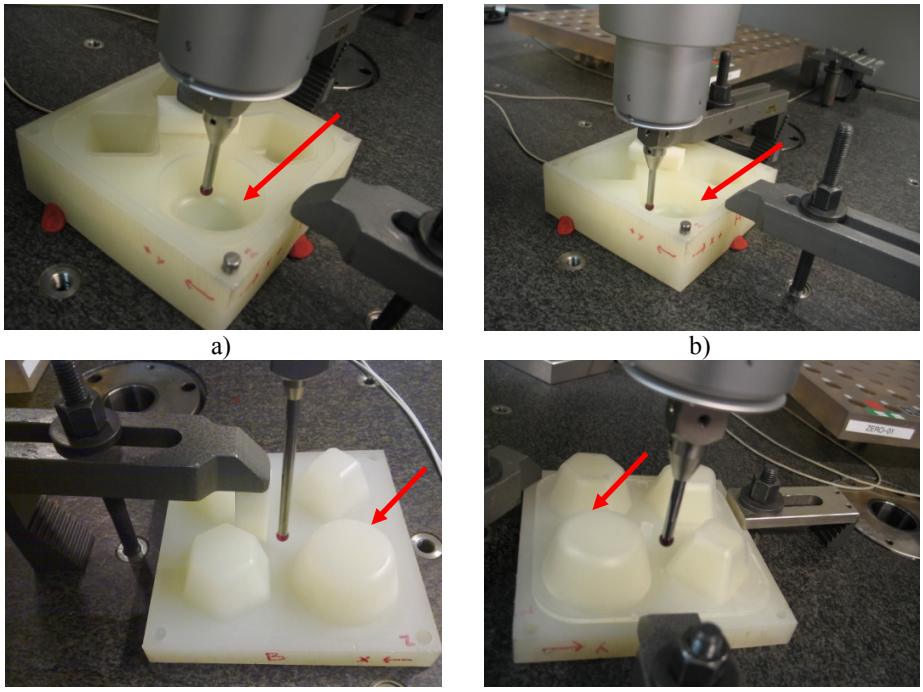

a) b) c) d)

Figure 5.1: Measurement setup for samples measured on tactile CMM: a) Form on A, b) Mold A, c) Mold B, d) Form on B.

5.2 TEST PLAN

A number of measurements using measuring instruments, described in Chapter 4, were realized. Table 5.2 presents the test plan and summarizes measurements performed both at DTU and DTI.

Table 5.2: Test plan.

Sample	CMM			Optical scanner	CT
	SPP	SMP	SPP (spheres)		
Form					x
Form on A	x				x
Form on B	x	x	x	x	x
Mold A	x				x
Mold B	x				x

5.3 DESIGN AND FIXTURING WITH A REFERENCE SYSTEM

In order to be able to compare individual measurements and their accuracy using different measuring techniques, both, single point probing (CMM) and a point cloud (optical scanner, CT scanner), must be referred to the same reference system with the minimum possible error. Several methods exist to perform this alignment [18] and [19].

The alignment was based on finding a point which is common to both parts of the molds, that is when they are in assembly. The reference point was established around the metal pin connecting both of the molds (Figure 5.2a and Figure 5.2b). After a plane was triggered around the cone in Z direction of the coordinate system, a new single point was probed nearby the pin to determine the zero in Z direction. This was due to the fact that the geometry (top surface) of the mold is not flat and variations in the Z plane were found. X-direction is defined on one side of the mold. A center of XY coordinate was defined as a center of the cone measured at a certain Z height.

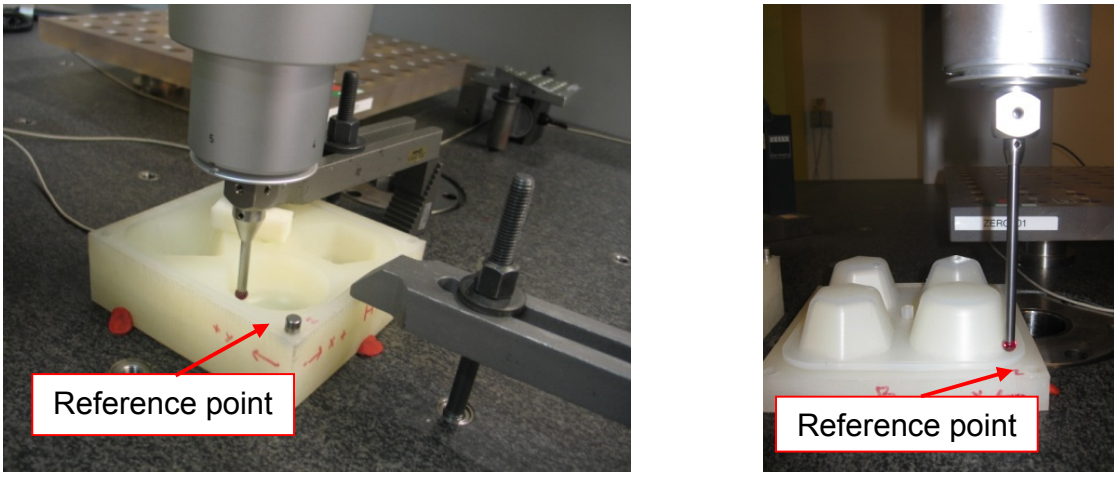

Figure 5.2: Position of the reference point on Mold A (a) and on Mold B (b). The reference point was defined around the metal pin connecting both parts (top and bottom) of the mold.

5.4 INVESTIGATION ON PROBING FORCE

The investigation of probing force effect on material deformation was performed on the CMM equipped with a static probe of a diameter of 8 mm.

The items investigated were:

- Form
- White form
- Mold A
- Mold B.

Both, Form and White form were measured alone, that is without a support of the Mold B, put on the granite table and with a support of the Mold B, which is a situation when both forms were put on the Mold B. In this setup, steel wedges were used to ensure stability of the silicone rubber on the supported molds and on the CMM table.

Four different forces were realized: 0.1 N, 0.2 N, 0.4 N and 1 N.

The measurement was performed in Z direction of the coordinate system, which is the direction of the probe perpendicular to the top surface of the samples. The smallest allowable force was set on the CMM, that is 0.1 N, and a zero point as an average of five repeated measurements was found. Then, measurements using other forces were performed and the deformation as an effect of the probing force was measured and compensated.

5.5 RESULTS

Naturally, when higher probing force was used, higher deformation of the material was measured. It can be seen from Figure 5.3 that the deformation is not influenced by the fact whether the forms were or were not supported by Mold B. Furthermore, the effect of the probing force on the deformation of the materials is linear, as predicted.

White form deforms more under the same probing forces than Form. This is due to the different material properties of both forms.

Deformation of the two molds result in much lower values compared to those measured on the two silicone rubber forms when the same probing forces were applied, see Figure 5.4. This is due to different material properties of the molds compared to forms materials.

Figure 5.5 shows the effect of the probing force on the coefficient of variation (*COV*). Parameter *COV* is calculated as follows:

$$COV = \frac{s}{a} \cdot 100\%$$

where

- *s* is the experimental standard deviation of five measurements
- *a* is the average of five measurements.

It can be seen that when bigger probing force is applied, the COV parameter decreases, meaning that the spread in values is smaller. Therefore, although a higher probing force creates higher deformation of the material, this results in a very stable performance which can be noticed from the small values of *COV* parameter.

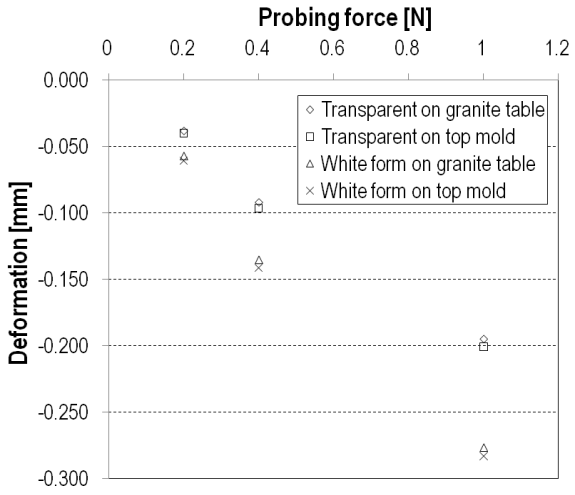

Figure 5.3: Deformation of the Form and White form.

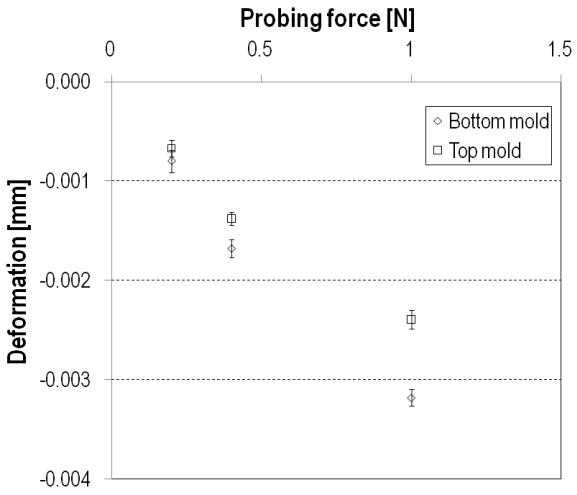

Figure 5.4: Deformation of the Mold A and Mold B.

5.6 MEASUREMENT SETUP AND MEASURING STRATEGY ON CMM

Measurements performed on CMM were realized using a probe of diameter of 8 mm and a probing force of 0.2N. All the measurements performed on CMM were reproduced three times. This includes measurements in

different days, repositioning of the mold from the granite table of the CMM, as well as repositioning of the Form from the mold.

Single point probing (SPP) and scanning mode probing (SMP)

Two different measurement strategies were realized for measurements on CMM. The first strategy considers diameter measurements using single point probing (SPP) method; the second one considers diameter measurements using scanning mode probing (SMP) method. The difference between these two types of measurement strategies is number of points which are realized around the cone circumference at individual height level. In the first case, 32 equally distributed points are probed on the circumference of the cone at individual levels. In the second case, number of points probed around the circumference is in the range 400-600, depending on the level measured. Number of probing points decrease with decreasing diameter of the cone at certain level.

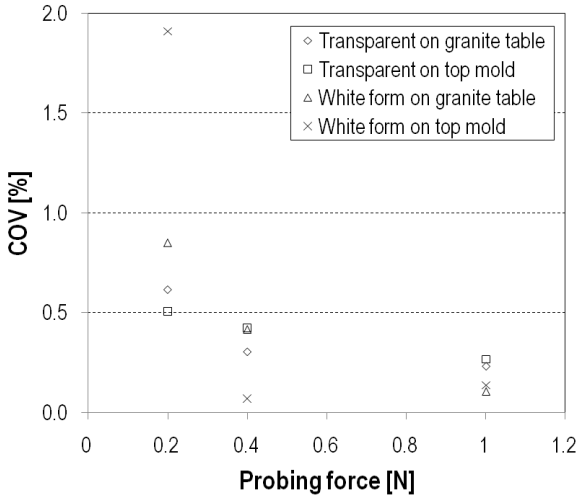

Figure 5.5: *COV* for the Form and White form.

For comparison between CMM and CT measurements, a diameter of the cone was measured at three given heights (-10, -15 and -20 mm for Form on A and 10, 15 and 20 mm for Form on B, with respect to Z-axis of the coordinate system), see Figure 5.6. Both, SPP and SMP were applied.

Due to the high elasticity of the transparent silicone rubber form, Form was measured on supported molds (Form on A, Form on B).

As it can be seen in Figure 5.1, the molds were clamped on the granite table of the CMM machine.

For comparison between CMM and optical measurements, a diameter of the cone was measured at three given heights of the cone (14, 16 and 18mm for Form on B with respect to Z-axis of the coordinate system), see Figure 5.7. As one can notice, these levels are different from the levels measured for comparison between CMM and CT. This was due to the fact that measurements on optical scanner did not allow measuring the cone in a bigger height range due to its complicated shape.

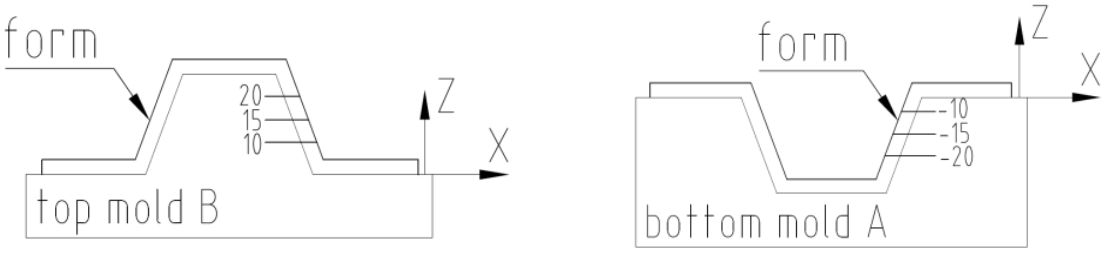

a) b)

Figure 5.6: Measuring strategy for Form on B (a) and Form on A (b), used to compare measurements on tactile CMM and CT scanner.

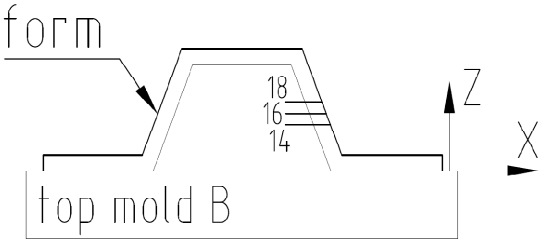

Figure 5.7: Measuring strategy for Form on B, used to compare measurements on tactile CMM and optical scanner.

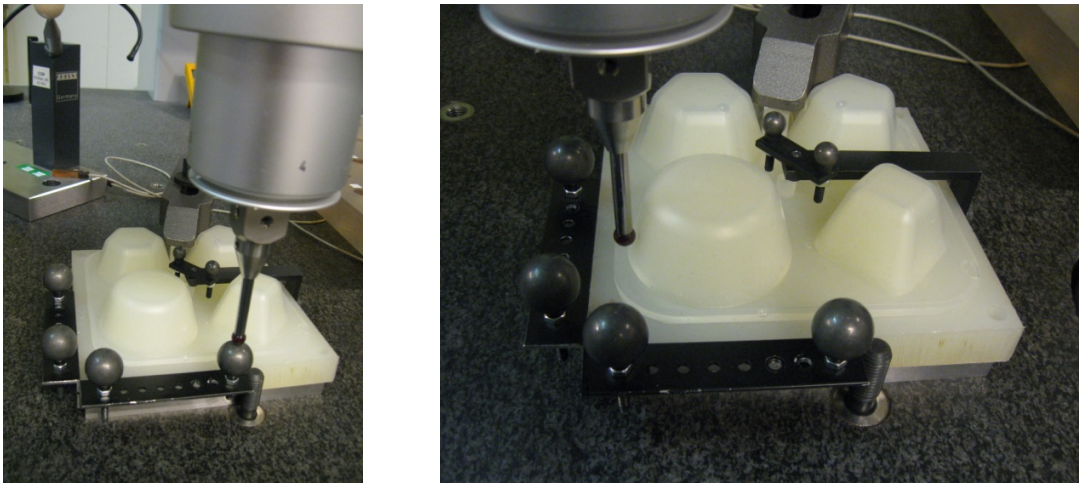

a) b)

Figure 5.8: a) Single point probing of the spheres; b) Single point probing of the cone.

As in the setup without the spheres, Form was measured on Mold B clamped on the granite table of the CMM machine (see Figure 5.9).

5.7 MEASUREMENT SETUP AND MEASURING STRATEGY USING OPTICAL 3D SCANNER

For the present investigation, Nextec Hawk was used. The Hawk DS 100 at DTU is equipped with a WIZprobe. Because the Form is not opaque, the molds were used as a support in order to acquire the points.

The sample investigated was the Form on B. The only feature scanned and measured was the cone of the Form. Five positions of the cone were established for scanning and in order to be able to stitch these five positions and measure subsequently, six spheres were mounted around the cone (Figure 5.9). For every position of the feature, three spheres were scanned at the same time.

The sample was mounted on the 3D motion platform, which consist of an XY motion stage, a Z axis arm which moves the WIZprobe, the electrical cabinet and the joystick. The stage contains M6 screw holes that are spaced at 25 mm intervals. Electric motors move the stage in the X and Y axes and it can be also moved through the use of the joystick. The sample was positioned approximately under 45° with respect to the XY table (Figure 5.10). This orientation of the sample allows the best acquisition of the points on the inclined surface.

The Swivel head (Figure 5.11) enables to adopt the orientation of the WIZprobe according to the object to be acquired. The head is adjustable along two axes (A and B) and lockable at intervals of 7.5°. The display of the head shows the orientation of the probe. For this case study, for each of five positions the calibrating tips chosen were A = 0° and B = 90°.

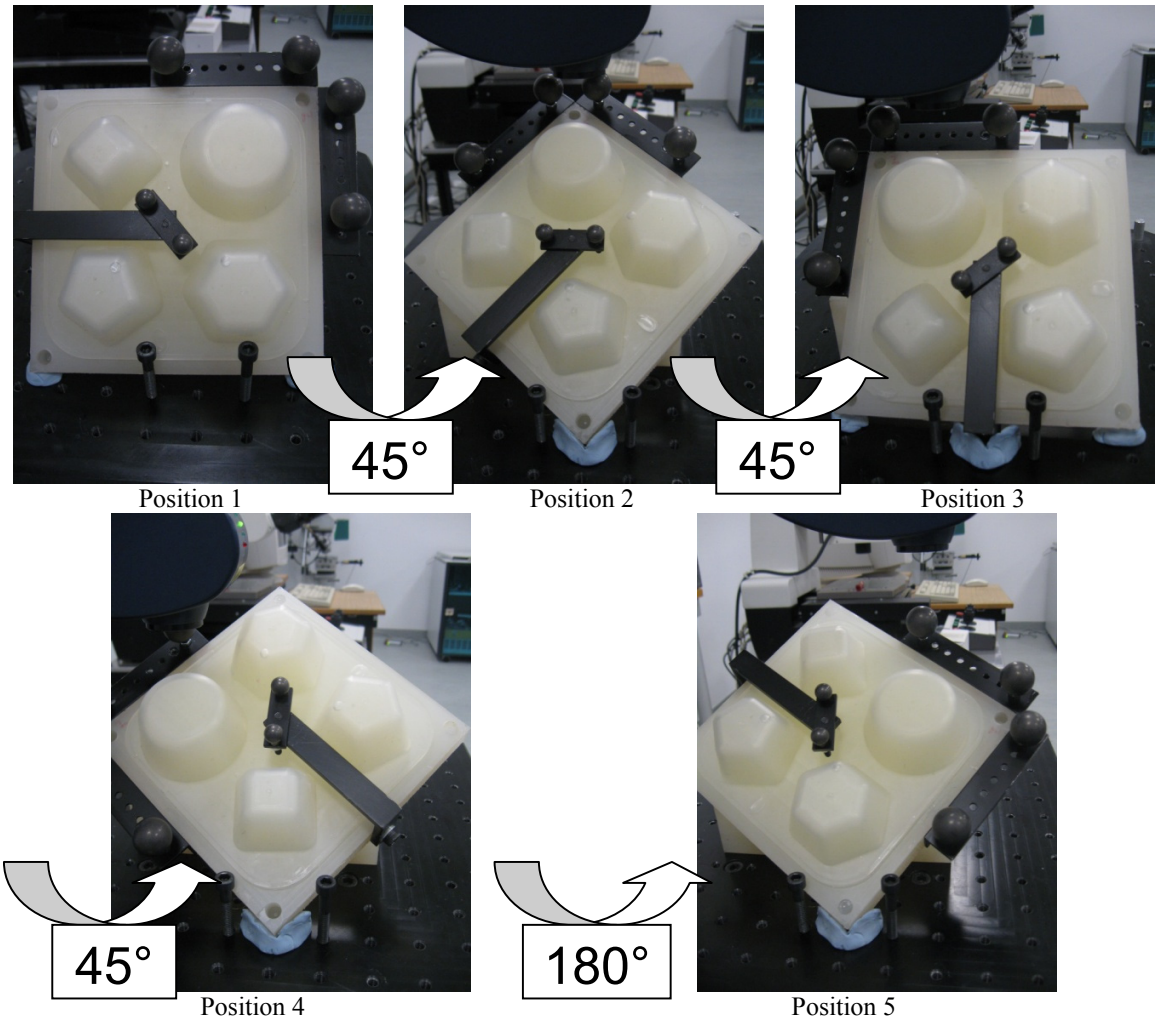

Figure 5.9: Measurement setup for all five position of the cone.

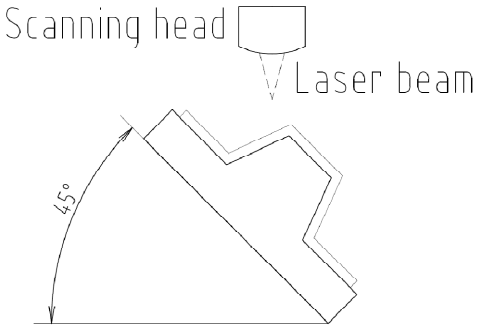

Figure 5.10: Sketch of a measuring setup for measurements using optical scanner.

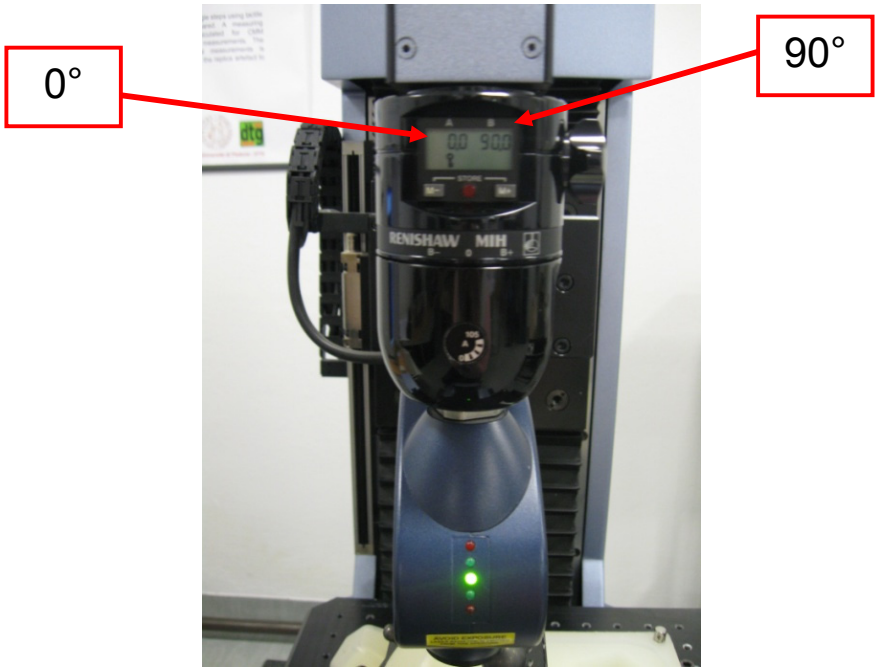

Figure 5.11: Swivel head positioning A = 0° and B = 90°.

The two inner green LEDs indicate that the allowable range is close and the middle green LED indicates optimum measuring range.

There are five scanning patterns available for defining point cloud: rectangle, arc, polyline, wideline and polygon. Each pattern performs the scan in a specific way. For acquisition of points on the cone of the Form, the rectangle pattern was used. To define the scanning area, three points were taken (Figure 5.12). This pattern runs the scan from point 1 to point 2 and continues as it is shown in Figure 5.13 until point 3. The distance *S* in the diagram refers to the Scanning Resolution and the distance *L* refers to Lateral Resolution. In this case study for scanning of the cone and the spheres, the scanning and lateral resolution were chosen to be 0.2 µm.

For defining point cloud of the spheres, the arc pattern was used. This pattern requires acquiring three points in order to define the scanning area. The schematic illustration of the principal for arc patters is shown in Figure 5.14.

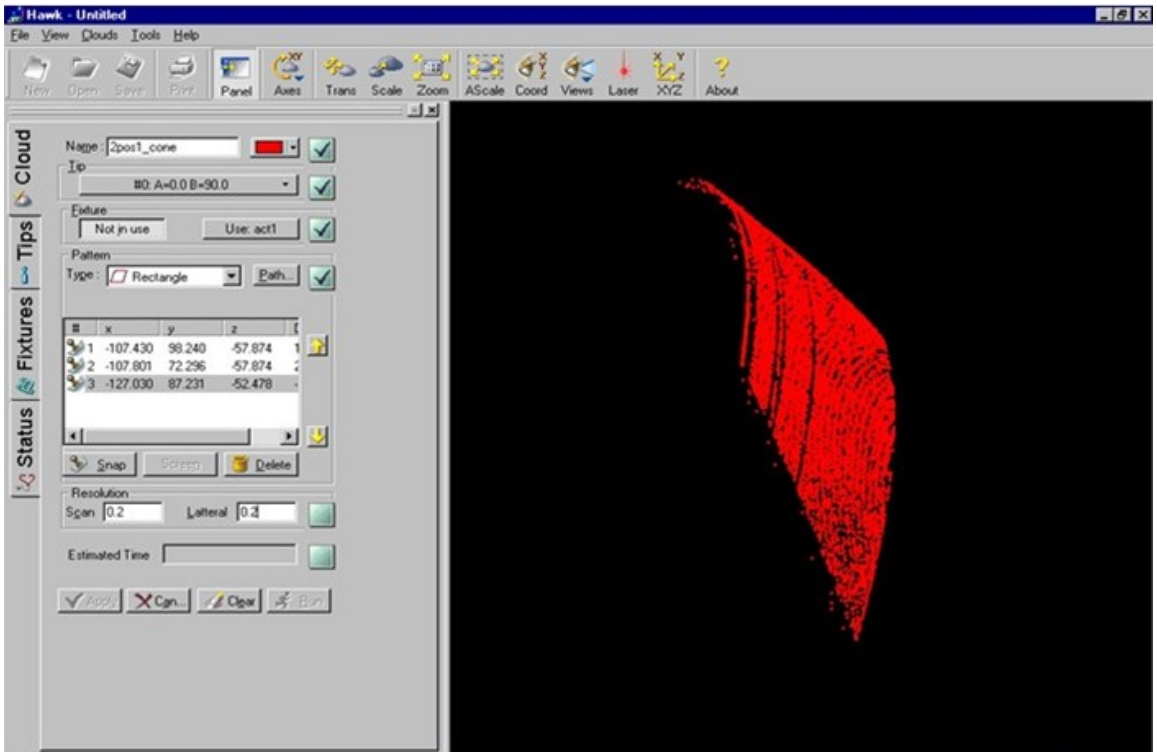

Figure 5.12: Screenshot of a window in Hawn software showing definition of acquired points on the cone. The path type was chosen to have a rectangular pattern for which three acquired points are needed. The scanning and lateral resolution was 0.2 µm.

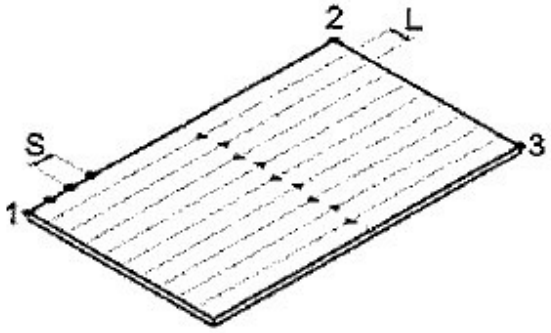

Figure 5.13: The rectangle pattern [20] defined by acquiring three points. *S* is scanning resolution and *L* is lateral resolution.

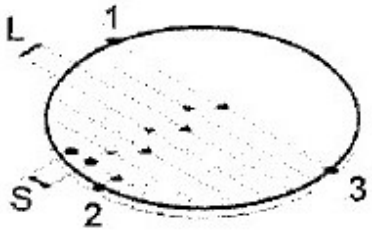

Figure 5.14: The arc scanning pattern [20].

Three reproduced measurements for each position of the cone were performed. Point clouds of the cone with specified number of spheres for all five positions can be seen in Figure 5.15. The red point cloud represents the scanned part of the cone and the other sphere-like objects of different colors represent the scanned spheres around the cone. Different colors are assigned to the same spheres at all five positions.

Diameters of the cone at three defined levels were investigated. The procedure for stitching of the five scanned positions is described as follows:

- Point cloud from the scanning on optical scanner is imported into ATOS software (see Figure 5.16).
- The point cloud is polygonized and saved as an STL file.
- Geometrical primitives (best fit spheres) are fitted to the polygonized scanned point clouds of the spheres (Figure 5.17).
- Line between spheres (sphere 1 and sphere 2 for position 1) and plane, based on three points (sphere 1, sphere 2 and sphere 4 for position 1), are constructed (see Figure 5.18).
- A 3-2-1 (plane-line-point) alignment, based on the previously created plane, line and sphere, is constructed with the origin in the center of sphere 1 (Figure 5.19).
- The same procedure is repeated for other four scanned positions.
- After all positions are stitched, points corresponding to the centers of the spheres measured by the CMM are created and using a 3-point alignment, these points are aligned to the centers of the spheres of the stitched configuration. In this way, diameter measurements at defined levels of the cone height can be performed.

Table 5.2 presents alignments for individual positions of the cone. One can see that the first three positions were aligned using the same spheres, whereas the other two positions used different spheres. When the first three positions were stitched together using the same alignment, a new alignment on this stitched configuration was created so that it could be stitched with a position 4. In the same way the last position 5 was stitched with previously stitched positions 1, 2, 3 and 4. This can be seen in Figure 5.20 which shows a cone stitching strategy for individual positions.

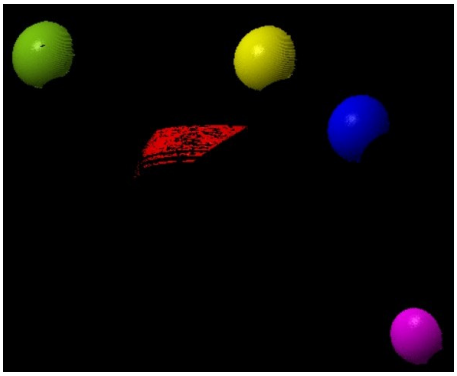

Position 1

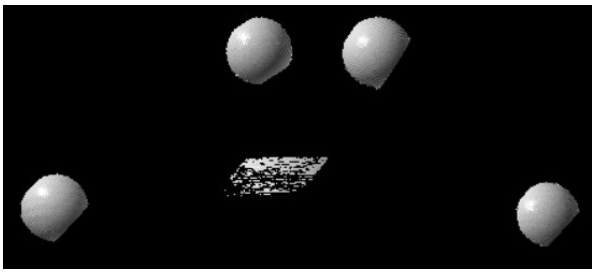

Position 2

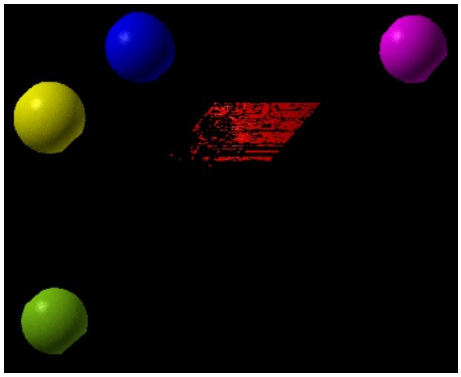

Position 3

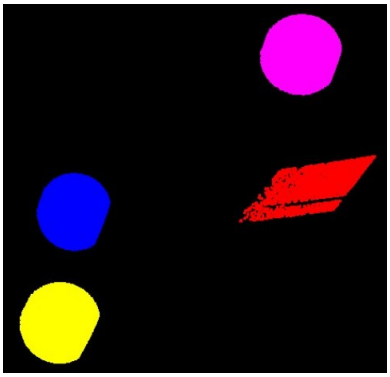

Position 4

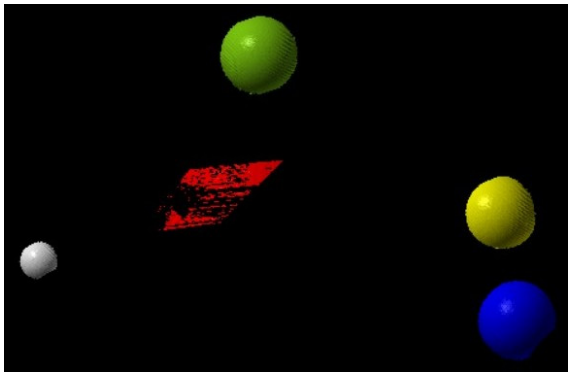

Position 5

Figure 5.15: Point clouds for all five positions of the cone and spheres.

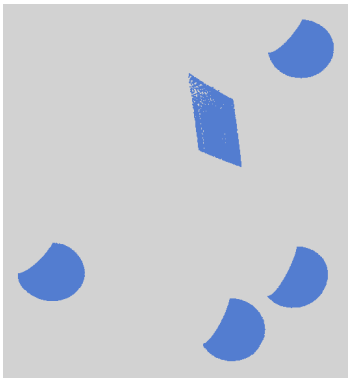

Figure 5.16: Original point cloud for position 1, scanned by optical scanner and imported in ATOS software.

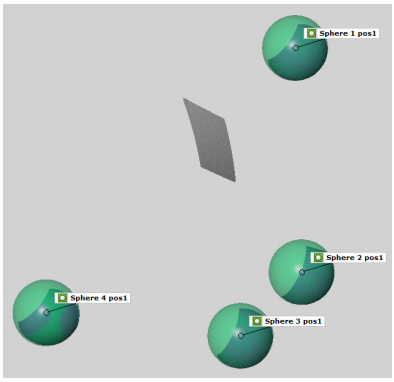

Figure 5.17: Polygonized scanned point cloud fitted to best fit spheres in ATOS software.

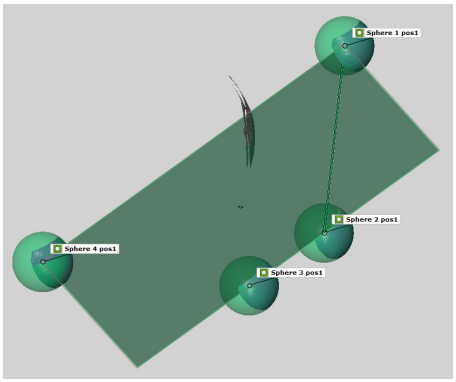

Figure 5.18: Line (between spheres 1-2) and plane (between spheres 1-2-4) constructed for the alignment.

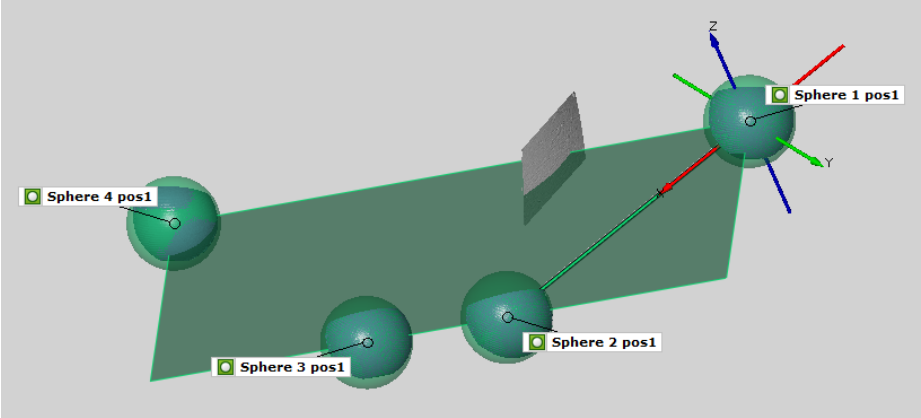

Figure 5.19: 3-2-1 (plane-line-point) alignment with the origin in the center of sphere 1.

Table 5.2: A 3-2-1 (plane-line-point) alignment for five positions used in ATOS software.

	3	2	1
Position	Plane	Line	Origin
	Sphere combination / Sphere number		
1	1-2-4	1-2	1
2	1-2-4	1-2	1
3	1-2-4	1-2	1
4	2-3-4	2-3	2
5	1-2-3	1-2	1

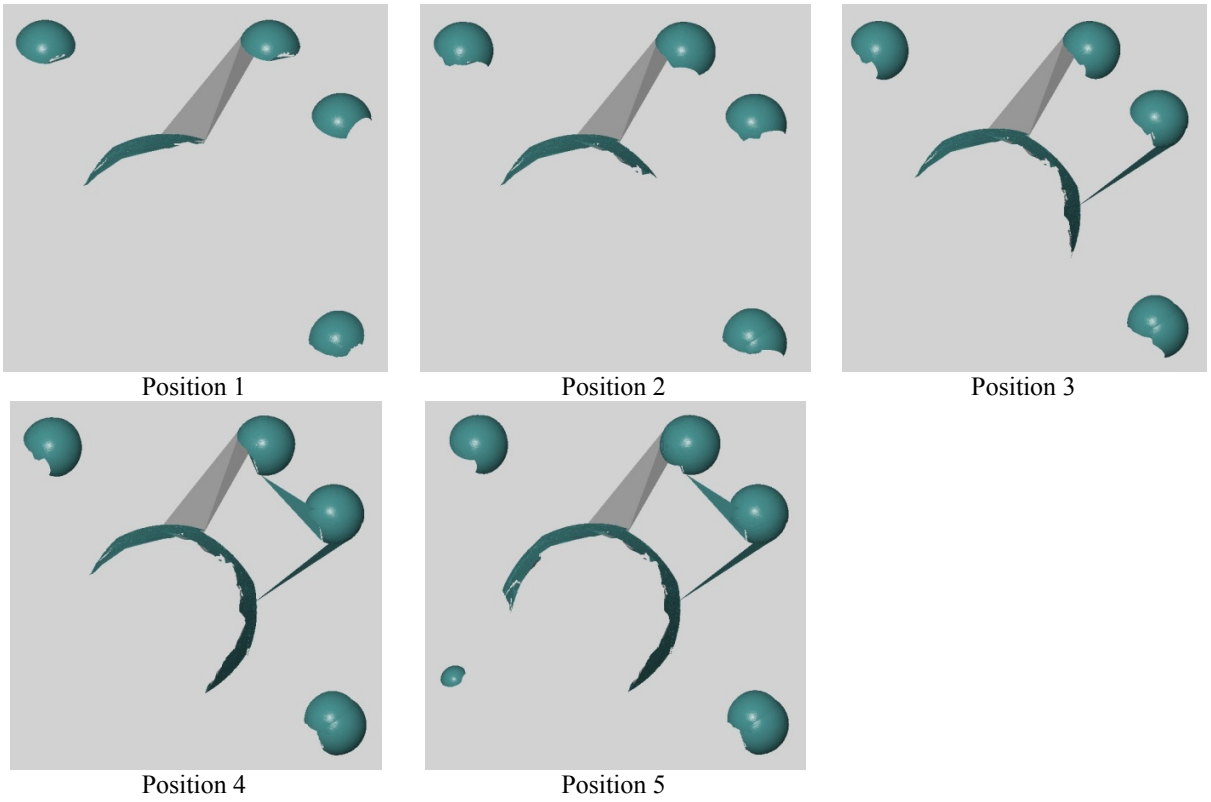

Figure 5.20: Stitching strategy for cone reconstruction, showing stitching of individual positions using spheres.

5.8 MEASUREMENT SETUP AND MEASURING STRATEGY USING CT

Both materials (silicone rubber form and polyamide molds) are suitable for measurements using CT. These materials are highly penetrable for X-rays to pass through and therefore allowing a reconstructed object in high contrast resolution.

During acquisition, the test parts were positioned on the rotary table of the CT scanner. When the Form was scanned, this was positioned horizontally with respect to the rotary table (Figure 5.21). The Form was attached to the polystyrene support using a double adhesive tape. This was used to ensure that the Form will not move during acquisition due to its high elasticity. In the case when the Form was scanned on Mold A and Mold B and the molds scanned separately, these were scanned under inclination of approximately 45° (Figure 5.22). This setup enables the best acquisition of the test part because in this way the length that the X-rays travel through the object is equally distributed along all angle positions.

The following samples were taken into account for measurements using CT scanner:

- Form
- Form on A
- Form on B
- Mold A
- Mold B.

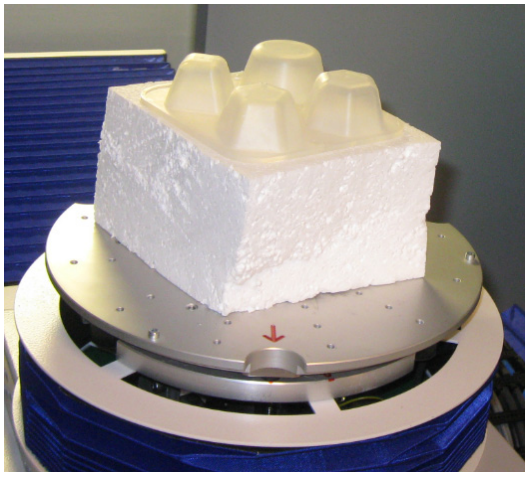

Figure 5.21: Positioning of the Form on the rotary table in CT scanner cabinet.

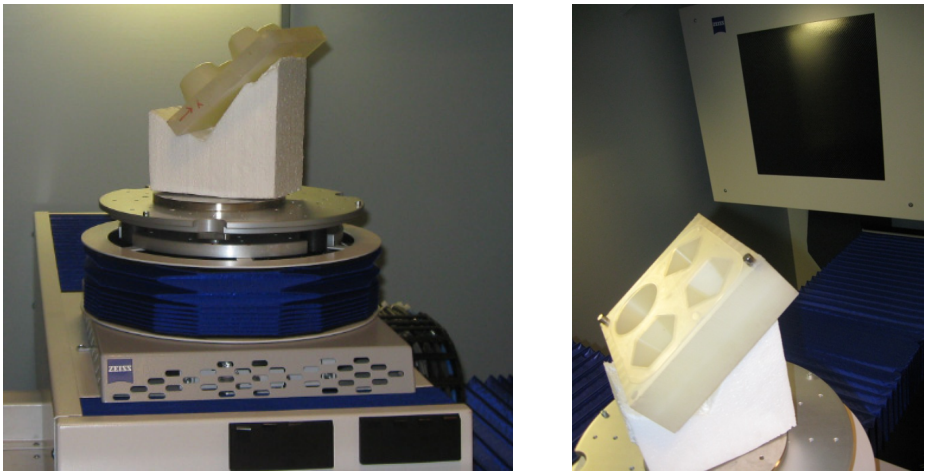

a) b)

Figure 5.22: Positioning of the Form on B (a) and Form on A (b) on the rotary table.

All the scans were reproduced three times. This takes into account measurements performed in the same days, taking the samples out from the cabinet of the CT scanner and put in again. In the case for scanning Form on A and Form on B, this was removed from the molds and put on again.

Previews of the scanned parts on the detector can be seen in Figure 5.23 and Figure 5.24. Moreover, Figure 5.23 shows a histogram of a gray scale distribution.

After the scanning of parts, the reconstruction of 2D projections (slices of the object) taken at a pre-defined angle step took place and a generated 3D model built up of voxels was obtained and ready for post-processing using CALYPSO CT software. The software is capable of translating gray levels of the voxels into point cloud. A generated 3D model can be seen in Figure 5.25a. The threshold value has to be carefully determined as it is a critical parameter for accurate image segmentation and surface data determination and thus has a great influence on the final geometry [21]. This step was set in CALYPSO CT software to be optimal since this software does not enable graphical segmentation of the object from the air. After that, surface of the measured object was generated and saved in STL format, see Figure 5.25b. This is based on creation of a surface made of triangles. The more triangles are

generated, the more precise measurements can be expected. The number of triangles was set in CALYPSO CT software to be optimal, too.

A diameter of the cone was measured on a generated STL model at three different height levels of the cone, at a nominal height 10mm, 15mm and 20mm in positive Z direction with respect to the coordinate system for both Mold A and Mold B (see Figure 5.6 in Chapter 5.6). Because of the geometry of the molds, the surface is not perfectly flat. This can be seen in Figure 5.26, which shows a fitted plane of the top surface of both Mold A and Mold B. Therefore, the selection of the Z plane plays a crucial role in comparison of diameter measurements performed on CMM. That is why the Z coordinate is created in the same way as in the case for tactile CMM. Selection on a defined area around the cone of the top surface of both molds was performed and a best fit plane was created. This can be seen in Figure 5.27. The scanning parameters can be seen in Table 5.4.

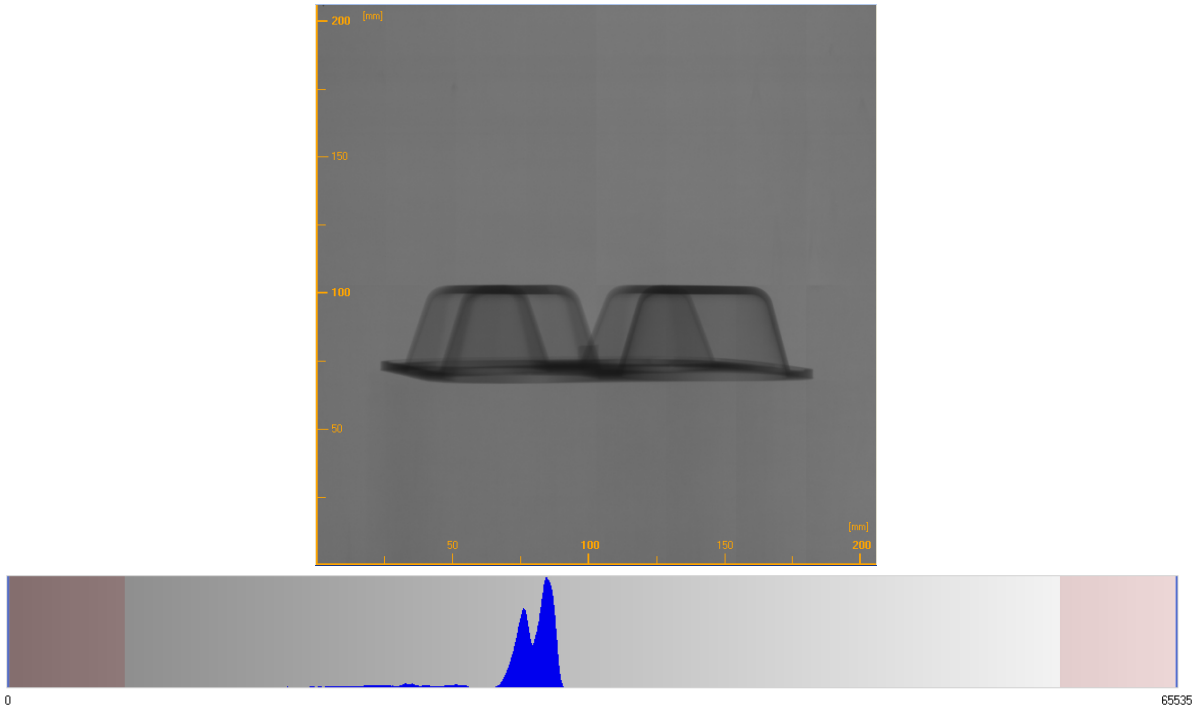

Figure 5.23: Projection of the scanned Form on the detector and a histogram of a gray scale distribution.

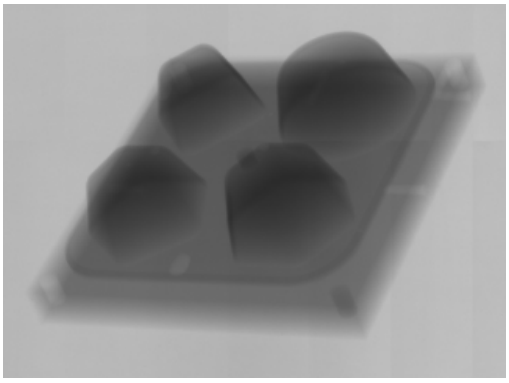

Figure 5.24: Projection of the scanned Form on B on the detector.

Table 5.4: Selected scanning parameters on CT scanner.

	Voltage	Current	FOD	Magnification
	kV	µA	mm	x
Mold A	150	150	870	1.72
Mold B	150	150	900	1.66
Form	150	150	450	3.3
Form on A	180	180	1000	1.5
Form on B	180	180	1000	1.5

Table 5.4: Selected scanning parameters on CT scanner - continued.

	No.of proj.	Voxel size	Source size	Integration time
	-	µm	µm	ms
Mold A	720	233	22	1000
Mold B	720	241	22	1000
Form	720	121	22	1000
Form on A	720	267	32	1000
Form on B	720	267	32	1000

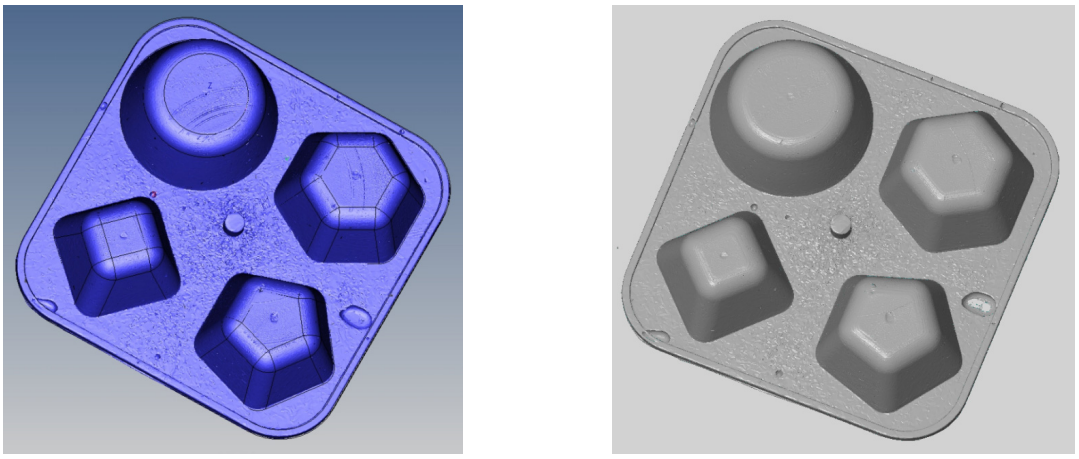

a) b)

Figure 5.25: A reconstructed 3D model of the Form (a) in CALYPSO CT software and extracted STL model of the Form in ATOS software (b).

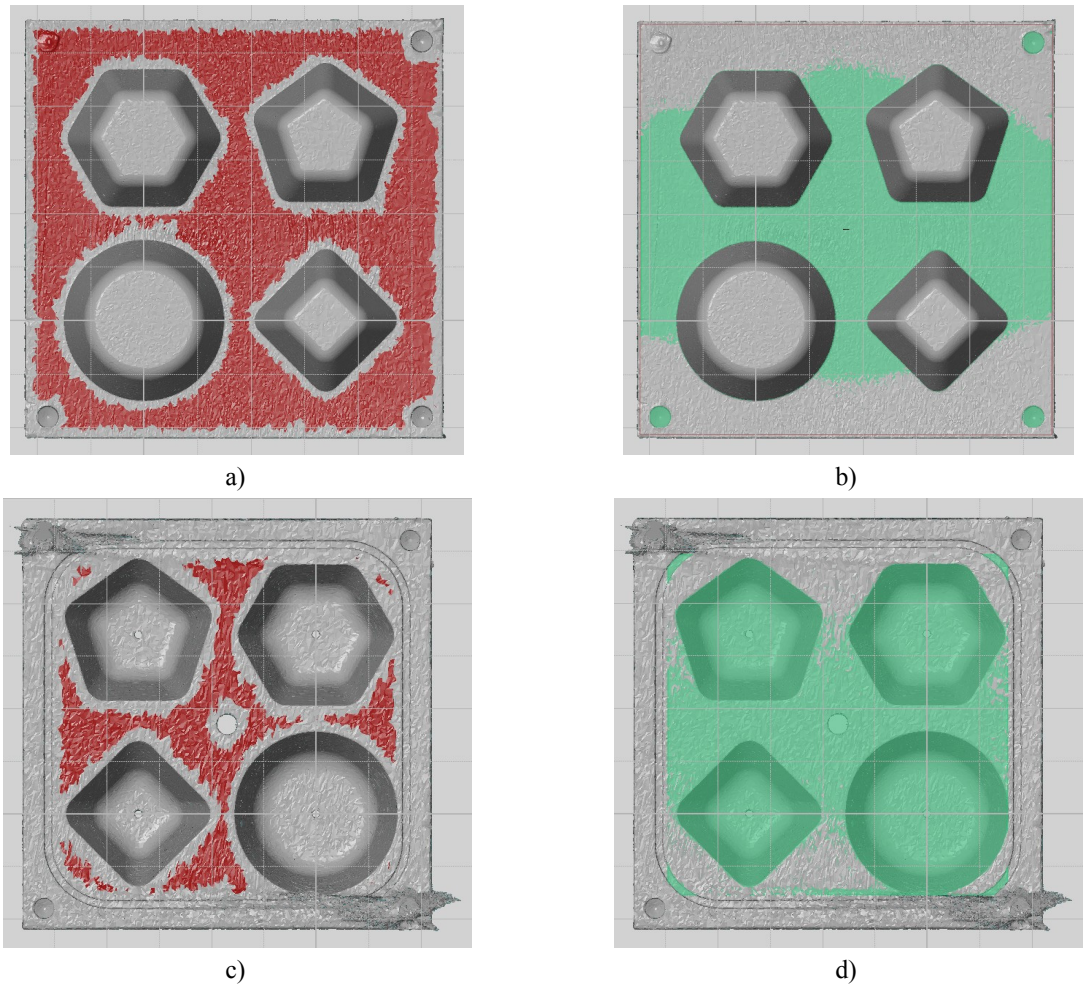

Figure 5.26: Variation of the surface on Mold B (a, b) and Mold A (c, d). By selecting the top surface of the mold (a, c), a best fit plane is created (b, d).

Moreover, a new zero point for Z coordinate was created, as in the case when measuring on tactile CMM (Figure 5.28).

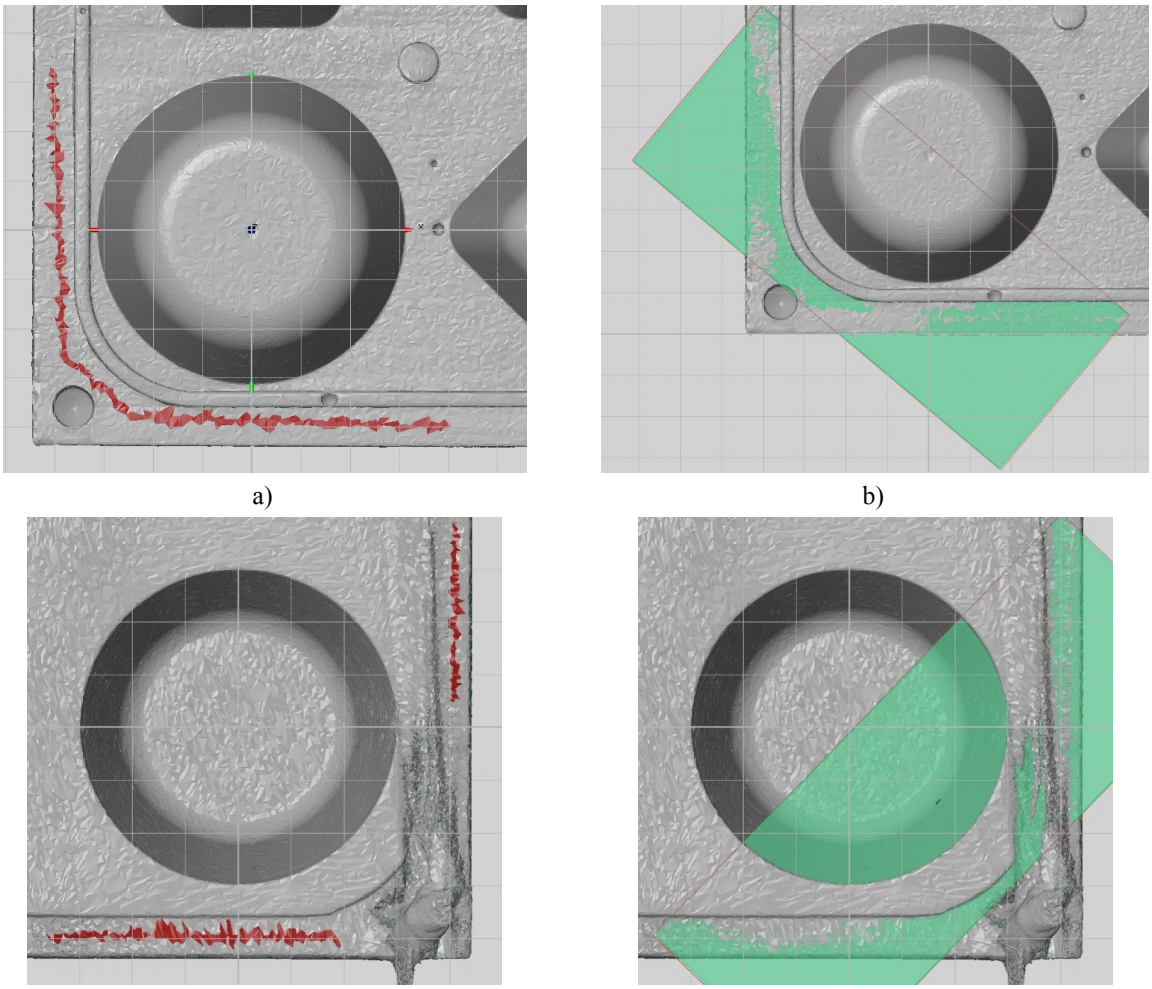

Figure 5.27: Definition of a plane in Z direction at the top face of Mold B (a, b) and Mold A (c, d) mold for measurements of the Form. By selecting flat features around the metal pin (a, c), a best fit plane is created (b, d).

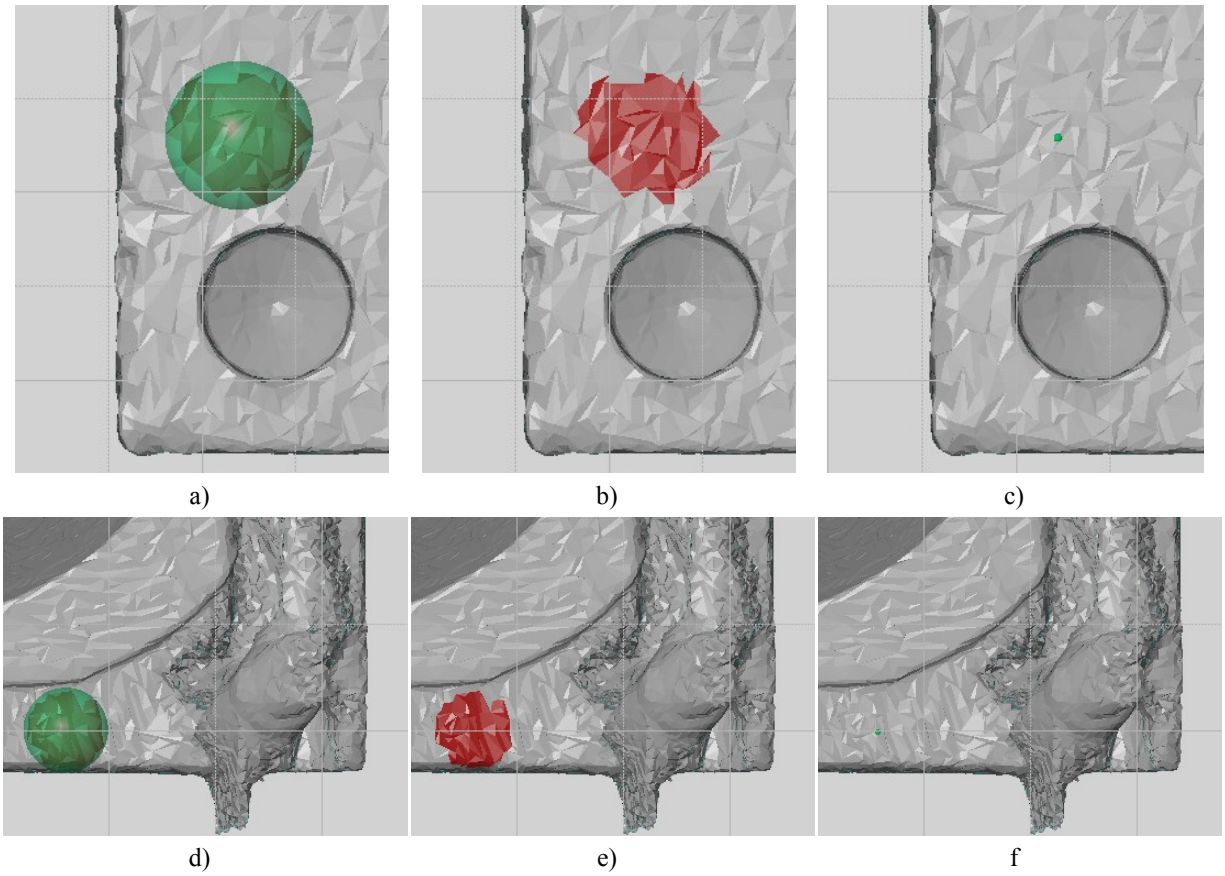

Figure 28: Creation of a new Z coordinate around the pin in ATOS software on the Mold B (a, b, c) and the Mold A (d, e, f) mold. Using select Inside Sphere selection method (the diameter of sphere for selection of points corresponds to a real probe diameter (a, d), the corresponding area is selected (b, e) and a best fit point is created (c, f).

Chapter 6

UNCERTAINTY ASSESSMENT FOR DIFFERENT MEASUREMENT TECHNIQUES

This chapter is dedicated to the uncertainty calculation. Uncertainty is calculated for each of the measuring techniques, using the GUM method [22], considering three uncertainty contributors for each technique. Assessment of measuring uncertainty in CT scanning is difficult due to many influence factors affecting the accuracy for dimensional measurement. Several studies were done in [12, 23, 24]. One of the valid approaches is to follow GUM procedures.

6.1 INTRODUCTION

According to [25], uncertainty is a parameter associated with the result of a measurement that characterizes the dispersion of the values that could reasonably be attributed to the measurand. Two characteristics are generally needed in order to quantify the uncertainty, these are:

- Interval, i.e. –U; +U
- Confidence level, i.e. statement about how sure one is that the true value is within the uncertainty interval. Usually, the level of confidence is 95%.

The importance occurs, when identifying all the sources which could contribute to uncertainty. Then the size of individual error sources has to be assessed. The error sources considered in the current investigation were due to:

- Instrument
- Environment (temperature)
- Reproducibility / repeatability of measurement.

6.2 UNCERTAINTY ASSESSMENT FOR MEASUREMENTS ON TACTILE CMM

The reference measurements were performed on tactile CMM, UPMC 850. Measurements were performed at the laboratory with controlled temperature. This is assessed to be 20 ± 0.5°C. The equation for uncertainty assessment is expressed as follows:

$$U = k \cdot \sqrt{u_{\text{inst}}^2 + u_{\text{env}}^2 + u_{\text{proc}}^2}$$

where

- U is expanded combined uncertainty

- k is Coverage factor (k=2 for confidence interval 95%)
- u_{inst} is standard uncertainty from the instrument
- u_{env} is standard uncertainty from the environment
- u_{proc} is standard uncertainty from the procedure (repeatability of the measurement)

Standard uncertainty related to the instrument:

$$u_{\text{inst}} = \frac{\text{MPE}}{2}$$

where

- MPE is Maximum Permissible Error of the machine; $\text{MPE}_{\text{CMM}} = (0.4 + L/900)$ µm, L in mm)

Standard uncertainty related to the environment:

$$u_{\text{env}} = \alpha \cdot \Delta T \cdot D_{\text{avg}} \cdot b$$

where

- α is coefficient of thermal expansion (CTE), CTE for silicone rubber form is $300 \cdot 10^{-6}$ $K^{-1}$and CTE for polyamide mold is $80 \cdot 10^{-6}$ K^{-1}
- ΔT is temperature variation during measurement (± 0.5 °C)
- D_{avg} is average measured diameter of a cone performed on three height levels of the cone, considering three repeated measurements
- b is a factor related to U-shape distribution (b=0.7)

Compensation of systematic error due to the temperature:

The temperature during the measurement changes and a deviation from the reference standard temperature of 20°C exists. This deviation causes an expansion that affects the measuring result with a systematic error, which has to be compensated. The compensation values taking into account both silicon rubber form and polyamide mold are calculated as follows:

$$\text{Comp(temp)} = \alpha_{\text{F}} \cdot \Delta T \cdot D_{\text{avg}}$$

$$\text{Comp(temp)} = \alpha_{\text{M}} \cdot \Delta T \cdot D_{\text{avg}}$$

The systematic effect on the diameter measurement is schematically illustrated in Figure 6.1. The systematic error due to the average temperature during measurements will be subtracted from the measurement result and the variation of this temperature, u, will be included in the uncertainty measurement, as earlier indicated as u_{env}.

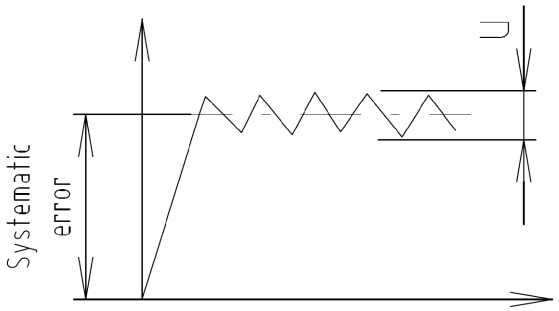

Figure 6.1: Systematic error due to the temperature.

Standard uncertainty related to the repeatability of the measurement:

$$u_{\text{proc}} = \frac{s_r}{\sqrt{n}} \cdot h$$

where

- s_{r} is average standard deviation of cone diameter measurements of three repeated measurements
- n is number of measurements
- h is safety factor (h=2.3 for three measurements)

6.3 UNCERTAINTY ASSESSMENT FOR MEASUREMENTS ON OPTICAL SCANNER

The measurements were performed on the optical scanner, Hawk DS 100, in a laboratory with average measured temperature of 21 ± 0.5°C. The equation for uncertainty assessment is expressed as follows:

$$U = k \cdot \sqrt{u_{\text{inst}}^2 + u_{\text{env}}^2 + u_{\text{proc}}^2}$$

where

- U is expanded combined uncertainty
- k is coverage factor (k=2 for confidence interval 95%)
- u_{inst} is standard uncertainty from the instrument
- u_{env} is standard uncertainty from the environment
- u_{proc} is standard uncertainty from the procedure (reproducibility of the measurement)

Standard uncertainty related to the instrument:

$$u_{\text{inst}} = \frac{res}{2}$$

where

- res is resolution of the optical scanner (res = 0.5 μm)

The assessment of other two uncertainty contributors (i.e. u_{env} and u_{proc}) is the same as in the case for tactile CMM.

6.4 UNCERTAINTY ASSESSMENT FOR MEASUREMENTS ON CT SCANNER

The measurements were performed on Metrotom 1500 CT scanner from Zeiss in a laboratory with average measured temperature of 21.5±1°C. The equation for uncertainty assessment is expressed as follows:

$$U = k \cdot \sqrt{u_{\text{inst}}^2 + u_{\text{env}}^2 + u_{\text{proc}}^2}$$

where

- U is expanded combined uncertainty
- k is coverage factor (k=2 for confidence interval 95%)
- u_{inst} is standard uncertainty from the instrument
- u_{env} is standard uncertainty from the environment
- u_{proc} is standard uncertainty from the procedure (reproducibility of the measurement)

The assessment of all three uncertainty contributors (i.e. u_{inst}, u_{env} and u_{proc}) is the same as in the case for tactile CMM. The only change is in the formula for MPE assessment for CT scanner, which is $\text{MPE}_{\text{CT}} = (9 + L/50)$ µm, L in mm).

Chapter 7

MEASURING RESULTS FROM CMM, CT SCANNER AND OPTICAL SCANNER

This chapter is dedicated to the comparison of the experimental results obtained with tactile CMM, optical scanner and CT scanner. First, two strategies (SPP and SMP) on CMM were compared. Secondly, comparison of results, considering cone diameter measurements at different height levels, between CMM and optical instrument and CMM and CT scanner was made. This only includes CMM measurements using SPP strategy.

7.1 COMPARISON BETWEEN SPP AND SMP STRATEGIES ON CMM

SPP measuring strategy in comparison with SMP strategy performed on CMM resulted in higher roundness. The roundness for SPP was 15 μm and 11 μm for SMP in average, considering three repetitions and three levels on the cone. Average standard deviation was calculated to be 2 μm for SPP and 0.7 μm for SMP. Figure 7.1 shows the average measured diameter comparison between SPP and SMP strategies.

Figure 7.1 shows individual contributions to uncertainty for all three uncertainty components as well as the expanded combined uncertainties for both strategies. It can be noticed that contribution due to the procedure is smaller for SMP strategy. Therefore, the expanded uncertainty at a confidence level of 95% is also lower for SMP. This contributor, u_{proc}, is however small compared to the uncertainty contributor due to environment. Small contribution of uncertainty due to procedure indicates very good reproducibility of measurement even on such a flexible part as silicon rubber form is. The biggest uncertainty contribution was due to the environment which is caused by variation of temperature and mainly due to high CTE of silicon rubber form.

7.2 CMM – OPTICAL SCANNER COMPARISON

The results of diameter measurements can be seen in Figure 7.2. It can be observed that the diameter of the cone at any of the levels results in higher values when measured using optical scanner. Individual points on the graph represent an average value of three reproducible measurements.

The standard deviation of measurements on CMM was 28 μm. It was investigated that the repeatability of the measurement using optical scanner is higher and is 103 μm.

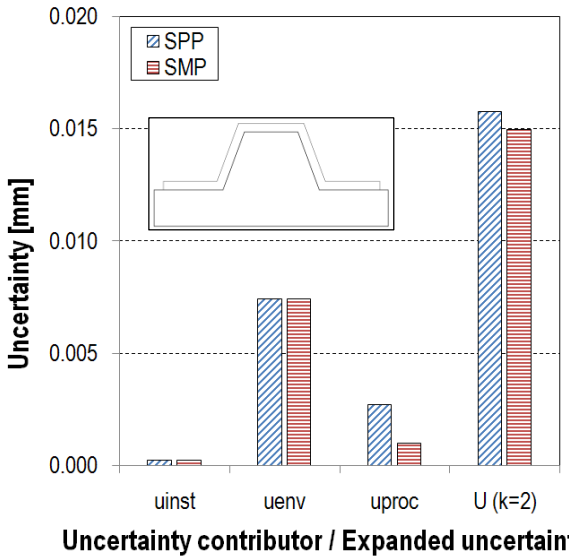

Figure 7.1: Uncertainty evaluation for measuring strategies SPP and SMP performed on tactile CMM for measurements of Form on B.

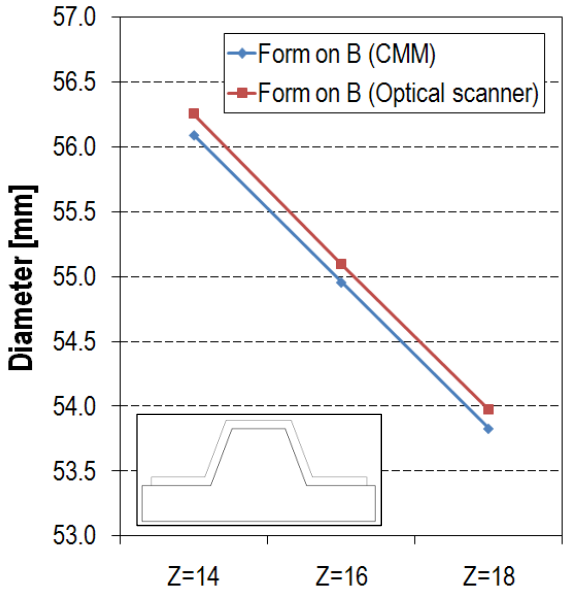

Figure 7.2: Diameter measurements of the cone for the Form on B performed on tactile CMM and optical scanner.

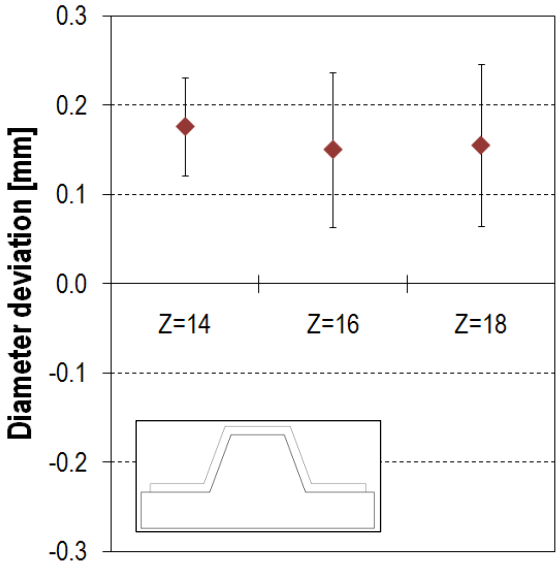

Figure 7.3: Measurements of diameter of the cone for the Form on B calculated as a difference between measurements performed on optical scanner and tactile CMM. The error bars represent experimental standard deviation at 1σ level.

As can be seen in Table 7.1, big uncertainty for measurements on optical scanner is mainly due to uncertainty contributors coming from the repeatability of the measurement, particularly from diameter measurement in ATOS.

Distance between individual spheres which were attached around the cone was measured by CMM and optical scanner. This is interpreted in Figure 7.4. Big deviations for distances where sphere 4 is considered are evident. This

is due to the imperfections which occur during scanning as is shown in Figure 7.5. It can be seen that the distances between individual spheres vary from position to position. Here, position represents an area where scanning of the cone was performed. As it was described earlier, five positions were scanned around the cone. It is interesting to notice from Figure 7.5a, that when stitching occurs, the distance is closer to the calibrated distances measured by tactile CMM. This is however not the case when distance between spheres 1 and 4 was measured (see Figure 7.5b). Big deviation from the calibrated values exists. That is why a big standard uncertainty due to the procedure was calculated for diameter measurements.

Table 7.1: Uncertainty evaluation for CMM and optical scanner performed on Form on B. All values in mm.

Uncertainty	Measuring instrument	
	CMM	Optical scanner
u_{inst}	0.0002	0.0002
u_{env}	0.0073	0.0073
u_{proc}	0.0376	0.1364
***U* (*k*=2)**	**0.0765**	**0.2731**

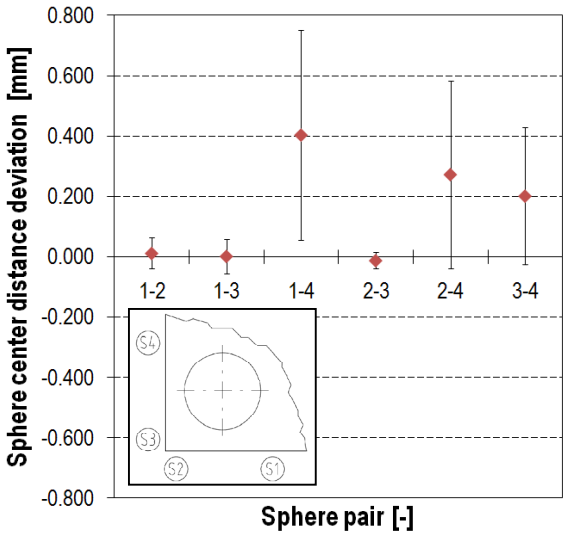

Figure 7.4: Comparison between sphere center distances measured by CMM and optical scanner. The error bars represent experimental standard deviation at 1σ level of three reproduced measurements.

Figure 7.6 shows a definition of the circle construction for diameter measurements in ATOS software. One can notice that the stitching of individual positions was not perfect and therefore results in big roundness measurements. The inner part of the circle in the figure probably belongs to Mold B which is used as support for the Form. This is probably due to the high transparency of the silicone rubber form.

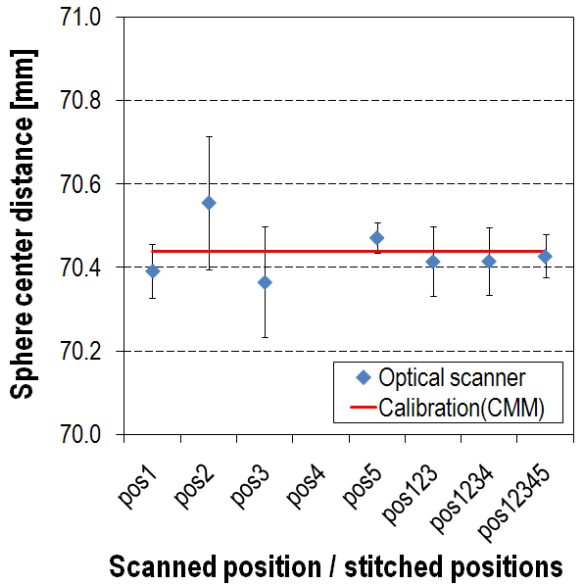

a) Distance comparison between Sphere 1 and sphere 2

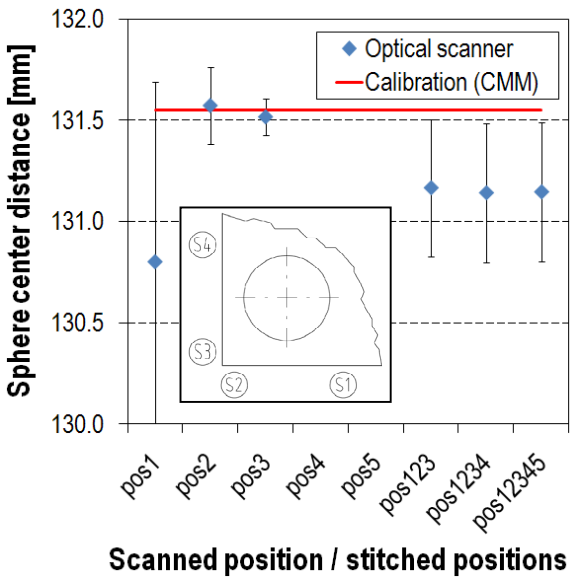

b) Distance comparison between Sphere 1 and sphere 4

Figure 7.5: Distance comparison between measurements performed on tactile CMM and optical scanner. The error bars represent experimental standard deviation at 1σ level based on three reproduced measurements.

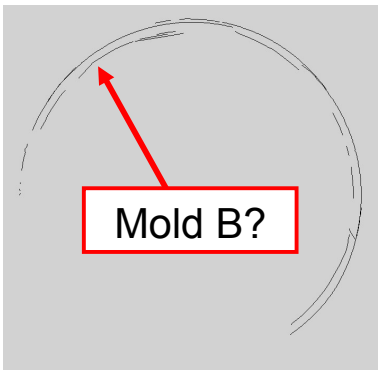

a) Poor quality of the stitched scanned positions of the cone seen at a cross-section of the cone.

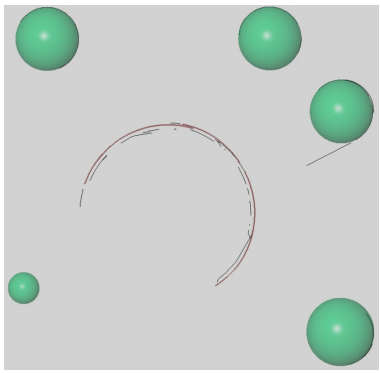

b) Selecting points on defined level of the cone.

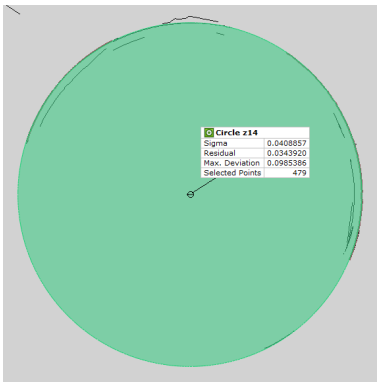

c) Fitting a best fit circle on the selected points.

Figure 7.6 Definition of the circle construction for diameter measurements in ATOS software.

7.3 CMM – CT COMPARISON

The results of diameter measurements for Form on B and Form on A can be seen in Figure 7.7. It can be observed that the diameter of the cone when the Form on B was measured bigger at any of the levels when measuring using CT scanner. When the Form on A was measured, the diameter of the cone at any of the levels was found smaller when measuring using CT scanner.

Figure 7.8 shows a diameter difference measured by the two measuring techniques. Individual points on the graph represent average values of diameter differences at three given levels (measurements of diameter for CT scans

are measured at the same Z level as in the case of CMM). It was experienced that the diameter measurements of the cone from CT scanner was smaller by 0.197 mm compared to measurements performed on the CMM when the form was measured on the supported top mold and the diameter of the cone was bigger by 0.267 mm in the case the form was measured on the supported bottom mold. This behavior was probably due to the determination of the threshold value. As it was shown for example in [46], threshold value changes in the opposite way for measurements of external and internal features.

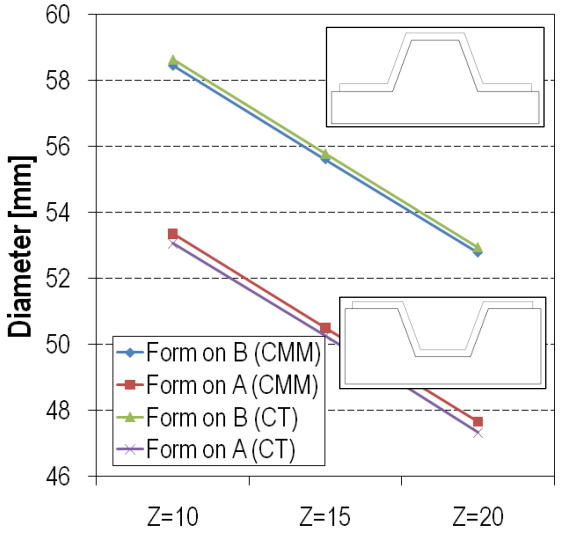

Figure 7.7: Diameter measurements of the cone for the Form on B and Form on A performed on CMM and CT scanner.

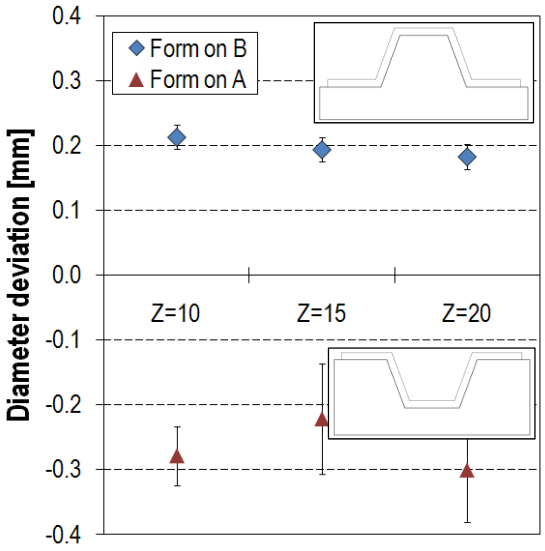

Figure 7.8: Measurements of diameter of the cone for the Form on A and Form on B calculated as a difference between measurements performed on CT scanner and tactile CMM. The error bars represent experimental standard deviation at 1σ level.

Table 7.2: Uncertainty calculation for Form on A and Form on B measured by CMM and CT scanner. All values in mm.

Uncertainty	Form on A		Form on B	
	CMM	CT	CMM	CT
u_{inst}	0.0002	0.0051	0.0002	0.0051
u_{env}	0.0067	0.0134	0.0074	0.0148
u_{proc}	0.0036	0.0903	0.0027	0.0247
***U* (*k*=2)**	**0.0152**	**0.1830**	**0.0158**	**0.0585**

Uncertainties for measurements on the CMM were for both cases, including measurements of the form on the supported top and bottom molds, calculated U (k=2) = 0.016 mm. Uncertainty of measurements on the CT scanner was calculated U (k=2) = 0.058 mm when the form was measured on the supported top mold and U (k=2) = 0.183 mm when the form was measured on the supported bottom mold (Table 7.2). Generally, measurements performed on CT scanner result in bigger uncertainties. Particularly, dominant are uncertainties connected with measuring procedures.

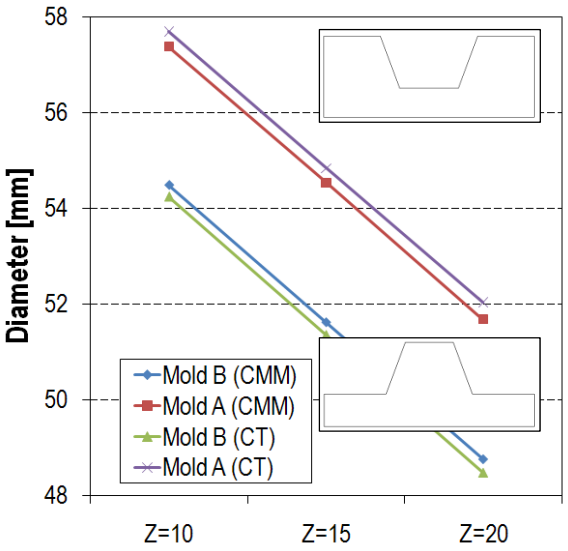

Figure 7.9: Diameter measurements of the cone for the Mold A and Mold B performed on CMM and CT scanner.

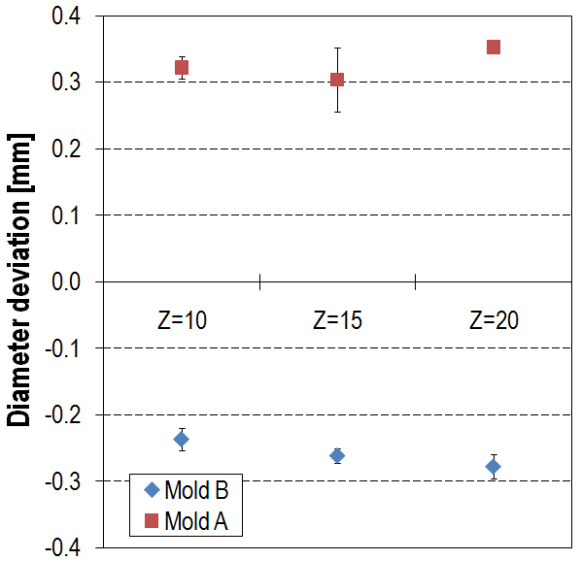

Figure 7.10: Measurements of diameter of the cone for the Mold A and Mold B calculated as a difference between measurements performed on CT scanner and tactile CMM. The error bars represent experimental standard deviation at 1σ level.

The results of diameter measurements for Mold A and Mold B can be seen in Figure 7.9. It can be observed that the diameter of the cone measured on Mold A by CMM at any of the levels results in smaller values compared to measurements performed on CT scanner. On the contrary, when the diameter of the cone was measured on Mold B by CMM at any of the levels, results in bigger values compared to measurements on CT scanner.

Figure 7.10 shows a diameter difference measured by the two measuring techniques. Individual points on the graph represent average values of diameter differences at three given levels (measurements of diameter for CT scans are measured at the same Z level as in the case of CMM), considering three reproducible measurements. One can also notice that the diameter deviation of Mold B is smaller than Mold A.

Table 7.3: Uncertainty calculation for Mold A and Mold B measured by CMM and CT scanner. All values in mm.

Uncertainty	Mold A		Mold B	
	CMM	CT	CMM	CT
u_{inst}	0.0002	0.0051	0.0002	0.0051
u_{env}	0.0073	0.0031	0.0069	0.0029
u_{proc}	0.0153	0.0232	0.0046	0.0187
***U* (*k*=2)**	**0.0339**	**0.0479**	**0.0165**	**0.0391**

Uncertainties for measurements on the CMM were for both molds found smaller than for CT measurements (Table 7.3). The difference was however not as significant as for measurements on Form on A and Form on B. This can be explained by better stability of the mold material (polyamide) compared to form material (silicone rubber). Therefore, smaller measuring variations (better reproducibility) are expected. It can be noticed from the table that uncertainty contributor related to measuring reproducibility was dominant, as in the case of measurements on the form.

A color map comparison of three reproduced CT scans of the Form can be seen in Figure 7.11. Here, each two CT scans are compared with each other. A requirement is that these scans have to be aligned in the same way. It can be noticed that a comparison between scan 1 and scan 2 (Figure 7.11 a, b) results in a good agreement, which is indicated by green color. This is also shown in the case of comparisons between scans 1-3 and 2-3 but only in the top view. From the bottom view of the Form, big deviations, represented by red color according to the scale on the right side, are presented. This behavior can be explained by dimensional changes of the sample during acquisition, maybe due to the temperature.

Color maps of three reproduced CT scans of the Form on A and Form on B can be seen in Figure 7.12 and Figure 7.13. Variations in the surface are shown. It can be observed that deviations of ± 0.5 mm are present for all the pairs of CT scans. One reason for this might be a misalignment of the samples in ATOS software since this is a difficult task to do on such samples with high flexibility and rough surfaces of the molds.

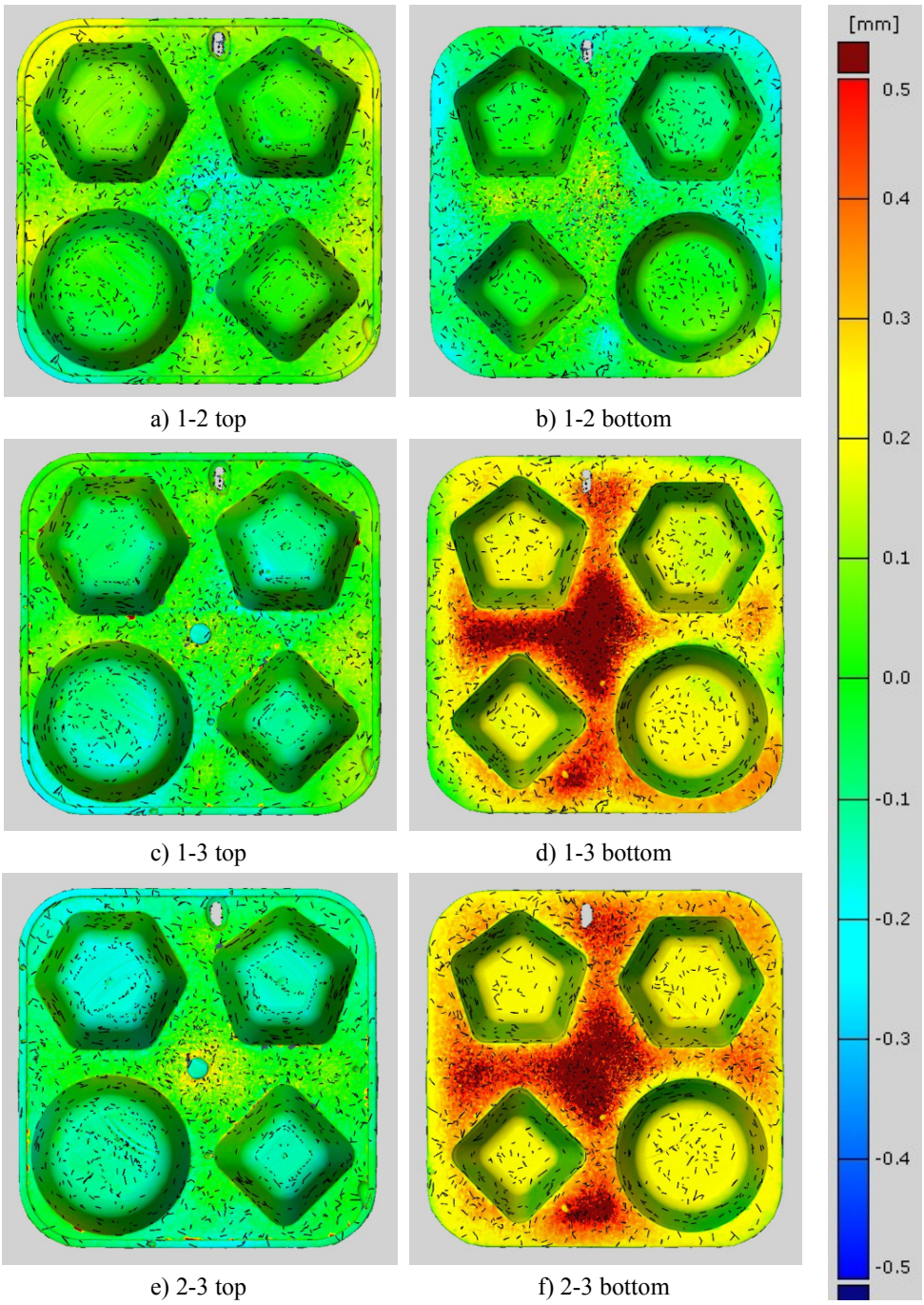

a) 1-2 top b) 1-2 bottom

c) 1-3 top d) 1-3 bottom

e) 2-3 top f) 2-3 bottom

Figure 7.11: Color map of three reproducible CT scans of the Form. The numbers, for example 1-2, represent comparisons between scan 1 and scan 2. Top view of the sample is shown on the left and bottom view of the sample is shown on the right.

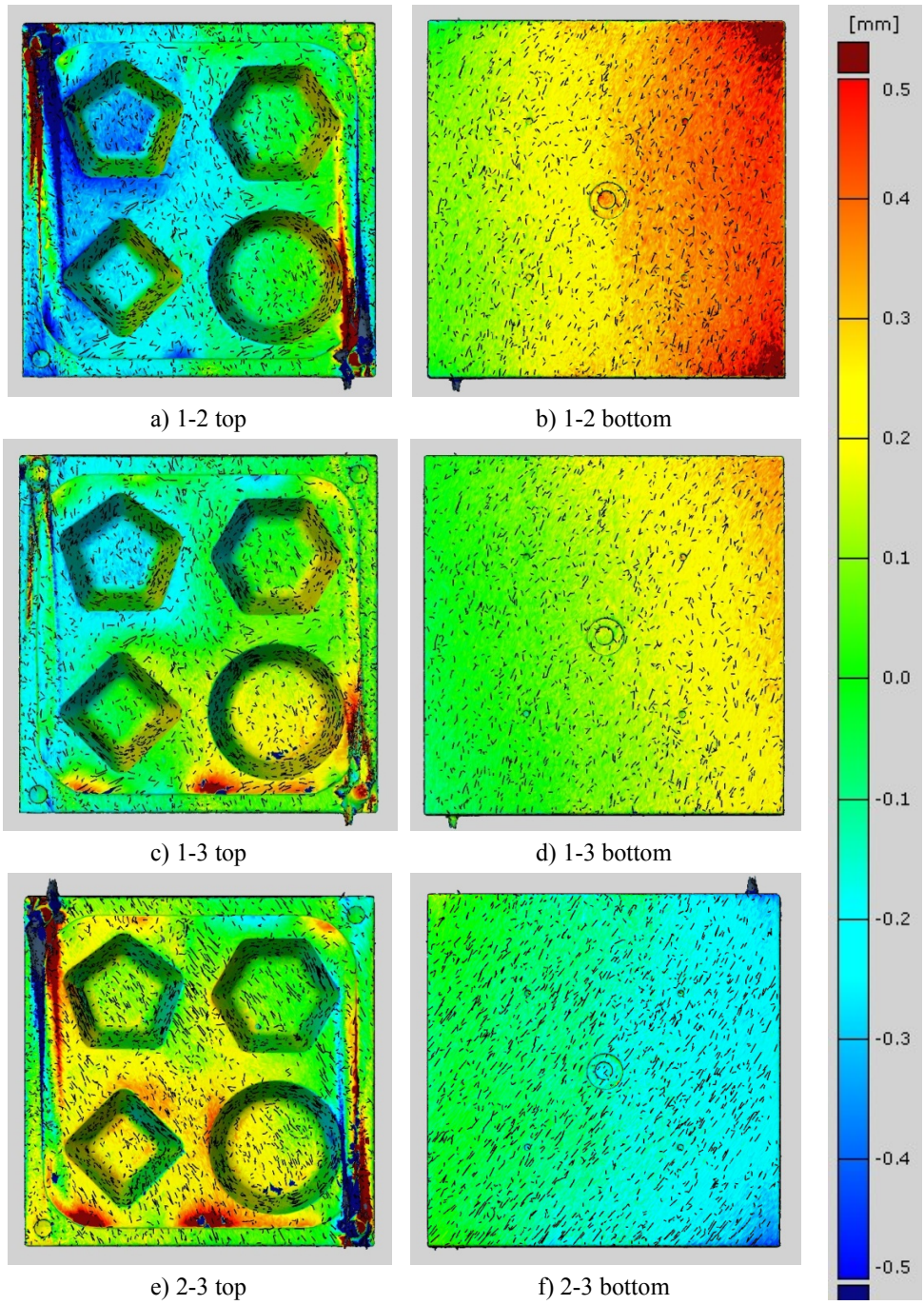

a) 1-2 top b) 1-2 bottom

c) 1-3 top d) 1-3 bottom

e) 2-3 top f) 2-3 bottom

Figure 7.12: Color map of three reproducible CT scans of the Form on A. The numbers, for example 1-2, represent comparisons between scan 1 and scan 2. Top view of the sample is shown on the left and bottom view of the sample is shown on the right.

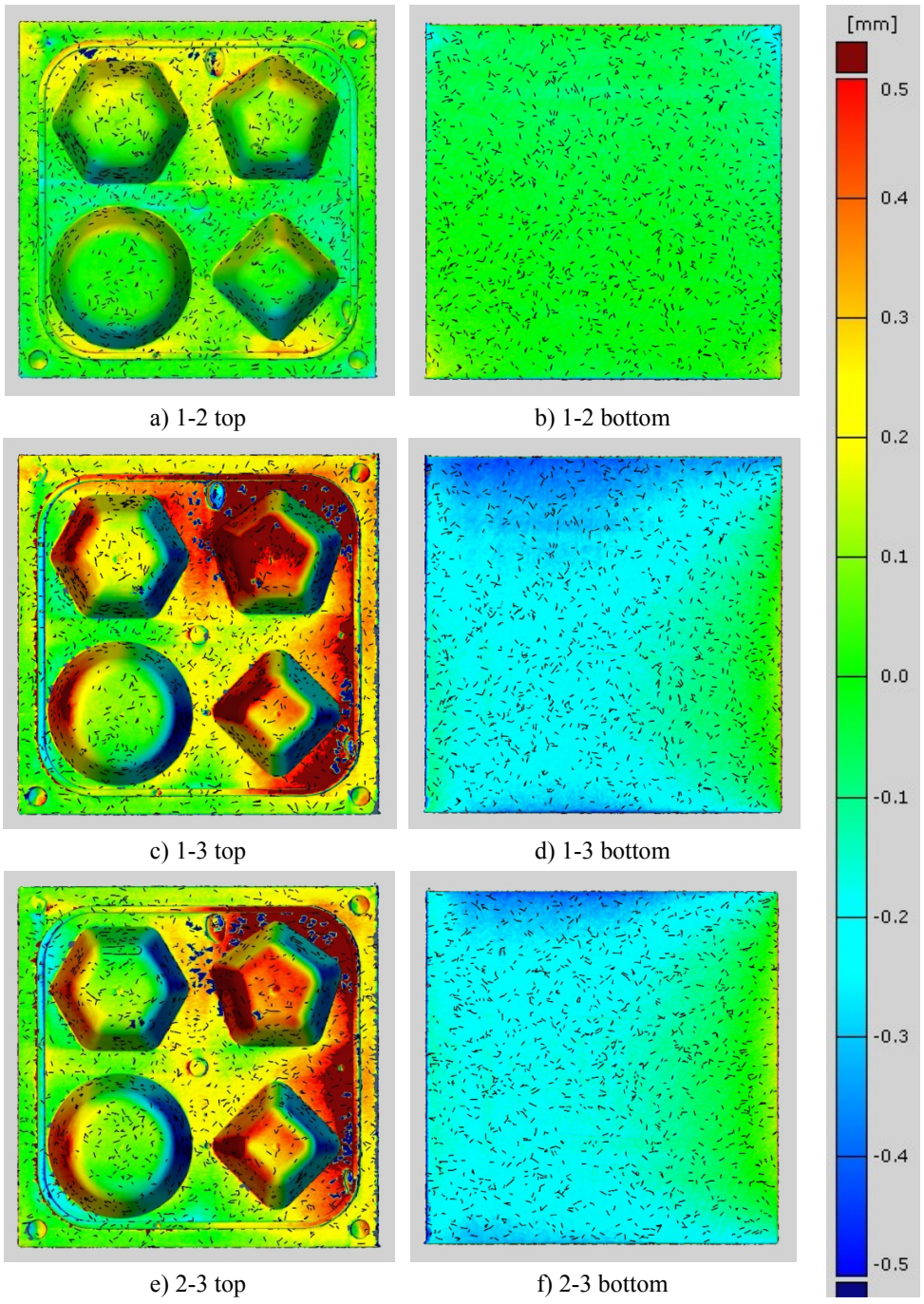

a) 1-2 top b) 1-2 bottom

c) 1-3 top d) 1-3 bottom

e) 2-3 top f) 2-3 bottom

Figure 7.13: Color map of three reproducible CT scans of the Form on B. The numbers, for example 1-2, represent comparisons between scan 1 and scan 2. Top view of the sample is shown on the left and bottom view of the sample is shown on the right.

Chapter 8

CONCLUSIONS

An investigation on geometrical measurements of silicone rubber cake form and polyamide molds using three measuring techniques - CMM, optical scanner and CT scanner - was carried out. The only measurand was diameter of a cone measured at specified levels. An uncertainty budget for all three techniques was assessed and expanded combined uncertainties calculated. The measurements on CMM were considered as reference measurements. The present investigation can be concluded with the following statements:

- It was found that when higher probing force was applied when measuring highly flexible silicone rubber form and polyamide molds, smaller coefficient of variation was obtained. This means that higher measuring reproducibility was achieved when higher probing force was applied.

- Comparing two measuring strategies (single point probing and probing in scanning mode) on CMM it was found that SMP results in smaller data variability. Because the difference in comparison with SPP measuring strategy was not big and since SPP measuring strategy is generally used for measuring a big variety of parts, SPP was used for further comparisons between CMM and the other two measuring techniques.

- It was found that when the silicon rubber form was measured on the supported bottom mold or the bottom mold was measured itself, the diameter measurements performed on optical scanner and CT scanner were bigger compared to CMM measurements. On the contrary, the diameter resulted in smaller values when the silicon rubber form was measured on the supported top mold or the top mold was measured itself.

- Uncertainties from measurement on the optical scanner were big. This was mainly connected with low reproducibility of scanning individual positions of the cone and difficulties when stitching individual parts of the cone. Measuring uncertainties for CT measurements were calculated in a range which is reasonable when considering such deformable sample. Therefore, one can say that CT scanning is highly recommended measuring technique, resulting in short measuring times and measuring of complicated features. In connection with the silicone rubber form, CT scanning could be also used for example for failure analysis, 3D volume analysis and other non-destructive and metrological analysis.

Chapter 9

OUTLOOK

Based on the results achieved in the present work, three suggestions on further research and development can be proposed.

a) Not only the cone of the silicon rubber form and both molds should be measured, but also other three features which form the cake form.

b) For product optimization of the silicon rubber form, a larger amount of forms is necessary to be produced and investigated.

REFERENCES

1. *http://en.wikipedia.org/wiki/Silicone_rubber*
2. Forrest, M.J. (2006). *Food Contact Rubbers: Products, Migration and Regulations*, Editura Rapra Technology Limited, United Kingdom, ISBN: 0889-3144.
3. *http://www.axson.fr/Front/downloads/essil-information_20080730173245.pdf*
4. De Chiffre, L. (2011). *Geometrical Metrology and Machine Testing*, Compendium Course 41731, DTU Mechanical Engineering.
5. *www.brownandsharpe.com/*
6. *www.cisimpex.ro/index-2.html*
7. *www.indiamart.com/ass-pvtltd/cmms.html*
8. *www.cimtrix.com/ml_atlas.htm*
9. Wilhelm, R.G., Hocken, R. And Schwenke, H. (2001). Task specific uncertainty in coordinate metrology, *Annals of CIRP*, **vol. 50/2**, pp. 553-563.
10. Martinez, S., Cuesta, E., Barreiro, J. and Alvarez, B. (2010). Analysis of laser scanning and strategies for dimensional and geometrical control, *International Journal of Advanced Manufacturing Technologies*, **vol. 46**, pp. 621-629.
11. Carmignato, S. (2005). Traceability of coordinate measurements on complex surfaces, *Ph.D. Thesis*, University of Padua and Technical University of Denmark.
12. Kruth, J.P., Bartscher, M., Carmignato, S., Schmitt, R., De Chiffre, L. and Weckenmann, A. (2011). Computed tomography for dimensional metrology, *CIRP Annals – Manufacturing Technology*, **vol. 60/2** (In Press).
13. Reinhart, Ch., (2008). Industrial computer tomography – a universal inspection tool, *17th World Conference on Nondestructive Testing*.
14. Bergmann, R.B., Bessler, F.T. and Bauer, W. (2004). Computer tomography for nondestructive testing in the automotive industry, *Proceedings of SPIE*, **Vol. 5535/1**, pp. 464-472.
15. *www.zeiss.com,* Zeiss, Industrial Metrology, Products.
16. Welkenhuyzen, F., Kiekens, K., Pierlet, M., Dewulf, W., Bleys, P., Kruth, J.P. and Voet, A. (2009). Industrial computer tomography for dimensional metrology: Overview of Influence Factors and Improvement Strategies, *4th International Conference on Optical Measurement Techniques for Structures and Systems*.
17. Franz, M., Funk, Ch., Hiller, J., Kasperl, S., Krumm, M., Schröpfer, S. and Ezrt, F. (2009). Reliability of dimensional measurements by computed tomography for industrial applications, *4th European-American Workshop on Reliability of NDE*.
18. Martínez, S., Cuesta, E., Barreiro, J. and Fernández, P. (2008). Testing the capabilities of the three - spheres alignment method for laser triangulation sensors, *6th international DAAAM Baltic conference*.
19. Van Gestel, N., Cuyperset, S., Bleys, P. and Kruth, J.P. (2009). A performance evaluation test for laser line scanners on CMMs, *Optics and Lasers in Engineering*, **vol. 47/3-4**, pp. 336-342.
20. Hawk User Manual, Nextec (2000).
21. Carmignato, S. (2007). Traceability of dimensional measurements in computed tomography, *In: Proceedings of 8th A.I.Te.M. Conference*, ISBN/ISSN: 88-7957-264-4.
22. ISO/IEC Guide 98-3:2008 - Uncertainty of measurement -- Part 3: Guide to the expression of uncertainty in measurement (GUM:1995).
23. Bartscher, M., Neuschaefer-Rube, U., and Wäldele, F. (2005). Computed tomography – a highly potential tool for industrial quality control and production near measurements.

24. Weckenmann, A. and Krämer, P. (2009). Assessment of measurement uncertainty caused in the preparation of measurements using computed tomography, *Fundamental and applied metrology, XIX IMEKO World Congress*, pp. 1888-1892, ISBN 978-963-88410-0-1.
25. ISO/IEC Guide 99:2007 - International vocabulary of metrology -- Basic and general concepts and associated terms (VIM).